Photo-oxidation of aromatic hydrocarbons produces low-volatility organic compounds

Mingyi Wang[1,2], Dexian Chen[1,3], Mao Xiao[4], Qing Ye[1,2], Dominik Stolzenburg[5], Victoria Hofbauer[1,2], Penglin Ye[6], Alexander L. Vogel[7], Roy L. Mauldin III[8,1,2], Antonio Amorim[9], Andrea Baccarini[4], Bernhard Baumgartner[5], Sophia Brilke[5], Lubna Dada[10], António Dias[9], Jonathan Duplissy[10,11], Henning Finkenzeller[12], Olga Garmash[10], Xu-Cheng He[10], Christopher R. Hoyle[4,13], Changhyuk Kim[14,15], Alexander Kvashnin[16], Katrianne Lehtipalo[10,17], Lukas Fischer[18], Ugo Molteni[4], Tuukka Petäjä[10], Veronika Pospisilova[4], Lauriane L. J. Quéléver[10], Matti Rissanen[19], Mario Simon[7], Christian Tauber[5], António Tomé[20], Andrea C. Wagner[7, 12], Lena Weitz[7], Rainer Volkamer[12], Paul M. Winkler[5], Jasper Kirkby[21,7], Douglas R. Worsnop[10,6], Markku Kulmala[10,11,22,23], Urs Baltensperger[4], Josef Dommen[4], Imad El-Haddad[4], and Neil M. Donahue[1,2,3,24,*]

[1]Center for Atmospheric Particle Studies, Carnegie Mellon University, Pittsburgh, PA 15213, USA; [2]Department of Chemistry, Carnegie Mellon University, Pittsburgh, PA, 15213, USA; [3]Department of Chemical Engineering, Carnegie Mellon University, Pittsburgh, PA, 15213, USA; [4]Laboratory of Atmospheric Chemistry, Paul Scherrer Institute, 5232 Villigen, Switzerland; [5]Faculty of Physics, University of Vienna, 1090 Vienna, Austria; [6]Aerodyne Research, Inc., Billerica, Massachusetts 01821, USA; [7]Institute for Atmospheric and Environmental Sciences, Goethe University Frankfurt, 60438, Frankfurt am Main, Germany; [8]Department of Oceanic and Atmospheric Science, University of Colorado Boulder, Boulder, CO 80309, USA; [9]CENTRA and FCUL, University of Lisbon, 1749-016 Lisbon, Portugal; [10]Institute for Atmospheric and Earth System Research (INAR), University of Helsinki, 00014 Helsinki, Finland; [11]Helsinki Institute of Physics, University of Helsinki, 00014 Helsinki, Finland; [12]Department of Chemistry & CIRES, University of Colorado Boulder, Boulder, CO 80309, USA; [13]Institute for Atmospheric and Climate Science, ETH Zurich, 8092 Zurich, Switzerland; [14]Division of Chemistry and Chemical Engineering, California Institute of Technology, Pasadena, CA 91125, USA; [15]Department of Environmental Engineering, Pusan National University, Busan, 46241, Republic of Korea; [16]Lebedev Physical Institute, 119991, Moscow, Russia; [17]Finnish meteorological Institute, Erik Palménin aukio 1, 00560 Helsinki, Finland; [18]Institute for Ion Physics and Applied Physics, University of Innsbruck, 6020 Innsbruck, Austria; [19]Aerosol Physics Laboratory, Physics Unit, Tampere University, P.O.Box 1001, Tampere, Finland; [20]IDL-University of Beira Interior, Covilhã, Portugal; [21]CERN, 1211 Geneva, Switzerland; [22]Joint International Research Laboratory of Atmospheric and Earth System Sciences, Nanjing University, Nanjing, China; [23]Aerosol and Haze Laboratory, Beijing Advanced Innovation Center for Soft Matter Science and Engineering, Beijing University of Chemical Technology, Beijing, China; and [24]Department of Engineering and Public Policy, Carnegie Mellon University, Pittsburgh, PA, 15213, USA.

[*]To whom correspondence should be addressed (Email: nmd@andrew.cmu.edu).

ABSTRACT

To better understand the role of aromatic hydrocarbons in new-particle formation, we measured the particle-phase abundance and volatility of oxidation products following the reaction of aromatic hydrocarbons with OH radicals. For this we used thermal desorption in an iodide-adduct Time-of-Flight Chemical-Ionization Mass Spectrometer equipped with a Filter Inlet for Gases and AEROsols (FIGAERO-ToF-CIMS). The particle-phase volatility measurements confirm that oxidation products of toluene and naphthalene can contribute to the initial growth of newly formed particles. Toluene-derived (C_7) oxidation products have a similar volatility distribution to that of α-pinene-derived (C_{10}) oxidation products, while naphthalene-derived (C_{10}) oxidation products are much less volatile than those from toluene or α-pinene; they are thus stronger contributors to growth. Rapid progression through multiple generations of oxidation is more pronounced in toluene and naphthalene than in α-pinene, resulting in more oxidation but also favoring functional groups with much lower volatility per added oxygen atom, such as hydroxyl and carboxylic groups instead of hydroperoxide groups. Under conditions typical of polluted urban settings, naphthalene may well contribute to nucleation and the growth of the smallest particles, whereas the more abundant alkyl benzenes may overtake naphthalene once the particles have grown beyond the point where the Kelvin effect strongly influences the condensation driving force.

INTRODUCTION

Organic condensation from the gas phase to the particle phase contributes to particle growth and causes secondary organic aerosol (SOA) formation [1]. SOA in turn may comprise well over half of the total fine-particle mass in the lower atmosphere, contributing to and possibly dominating health effects include more than 4 million premature deaths per year [2,3]. However, to what extent organic condensation affects the initial growth of nucleated particles remains in doubt, and the mechanism forming "condensable" organic vapors is even less certain [4]. The growth rate of freshly nucleated particles is crucial to their survival [5], which in turn governs the connection between particle nucleation and aerosol-cloud interactions, one of the most uncertain elements of the climate system [6].

Recent results from the “Cosmics Leaving OUtdoor Droplets” (CLOUD) experiment show

that organic vapors emitted by trees can produce abundant aerosol particles through nucleation of ultra-low volatility organic compounds (ULVOCs) even when there is no sulfuric acid [7]. Tröstl *et al*. [1], Lehtipalo *et al*. [8] and Stolzenburg *et al.* [9] have constrained the role of pure biogenic organic vapors in the initial growth of nucleated particles via laboratory experiments free from inorganic acids and bases or nitrogen oxides (NO_x). Combined experimental data and model simulations show that biogenic organic vapors driving initial growth up to ~2 nm are extremely low-volatility organic compounds (ELVOCs). As particles grow and the Kelvin effect diminishes, subsequent growth is taken over by more abundant low-volatility organic compounds (LVOCs) with slightly higher volatility [10].

Ozonolysis of terpenes, followed by peroxy-radical autoxidation via a succession of internal H-atom transfer reactions, produces ULVOCs and ELVOCs within a few seconds after the initial attack by ozone [11]. This drives new-particle formation in regions dominated by biogenic emissions [12]. However, these processes can be suppressed substantially in polluted airmasses, where nitrogen oxides (NO_x) can perturb peroxy-radical chemistry and suppress ULVOC and ELVOC formation [13]. Further, even under optimal conditions, those compounds comprise only < 5% of the terpene oxidation products [14]. Though first-generation auto-oxidation plays a major role, the (large) balance of "traditional" product vapors cannot be neglected; those vapors will undergo further oxidation, which has been shown to increase yields of SOA [15] and also to form more ELVOCs via subsequent autoxidation [16].

Pollution contains much more than NO_x. In the urban atmosphere, aromatic hydrocarbons can account for up to 60 % of the total VOCs [17,18]. Among them, small monocyclic aromatics are mostly emitted from anthropogenic sources, such as fossil-fuel combustion and solvent evaporation, with toluene being one of the most abundant species [17,18]. Polycyclic aromatic hydrocarbons mainly come from incomplete combustion such as heavy-duty diesel vehicles, biomass burning and meat cooking [19–21]; formation of naphthalene is often favored among PAHs during these combustion processes [20]. Aromatic hydrocarbons are believed to play a critical role in the formation of both tropospheric ozone and secondary organic aerosols (SOA) [22–25]. Laboratory studies have also reported highly oxygenated product formation from OH-triggered oxidation of aromatic hydrocarbons, highlighting their potential contribution to nucleation and initial particle growth in the anthropogenic environment [26,27].

Despite the significance of aromatic systems to the urban atmosphere, the volatility profile of oxidation products from aromatic precursors has yet to be established. The contribution of aromatic-derived oxidation products to urban new-particle formation has so far remained ambiguous. Here, we extend previous CLOUD experiments on biogenic organic vapors to add toluene and naphthalene as examples of anthropogenic organic vapors, comparing the formation pathways of oxidized organics as well as their behaviors on contributing to the growth of newly formed particles in the urban environment.

MATERIALS AND METHODS

We conducted experiments involving aromatic precursors under typical urban conditions in the "Cosmics Leaving OUtdoor Droplets" (CLOUD) chamber. The CLOUD facility was constructed to measure nucleation and growth rates of inorganic and organic vapors under highly controlled, ultra-clean conditions. The 26.1 m^3 stainless steel chamber is kept scrupulously clean, with background contaminants (H_2SO_4, organics, amines) < 10^5 cm^{-3}. It can be exposed to ultraviolet (UV) light via a fiber-optic system to generate OH radicals uniformly via ozone photolysis, initiating subsequent photochemical reactions. In addition, the Xe arc lights with UVA at 385 nm from a set of 400 W LED lights are augmented to photolyze NO_2 to NO. The chamber temperature can be controlled from 183 to 373 K [28], and relative humidity (RH) from < 0.5% to 101%, enabling experiments over a wide range of tropospheric conditions.

Experiment conditions. Results presented here are from the CLOUD-11 campaign in Fall 2016. To simulate urban environments, we fixed the temperature at 20 ℃, relative humidity at 60%, ozone concentration at ~ 40 ppbv, NH_3 concentration at ~ 500 pptv, SO_2 concentration at ~ 2 ppbv, and NO_2 concentration at ~ 1−2 ppbv. We conducted experiments with different aromatic precursor concentrations spanning urban conditions − 8 ppbv and 40 ppbv for toluene and 2 ppbv and 15 ppbv for naphthalene. We formed OH radicals via ozone photolysis and the subsequent reaction of $O(^1D)$ with water vapor.

Chemical ionization mass spectrometer. We measured the gas-phase and particle-phase composition as well as particle-phase volatility of oxidation products via thermal desorption using an iodide-adduct Time-of-Flight Chemical Ionization Mass Spectrometer equipped with

a Filter Inlet for Gases and AEROsols (FIGAERO-ToF-CIMS). Iodide-adduct chemical ionization is well suited for measuring a suite of oxygenated organics with minimal fragmentation [29]. The FIGAERO is a manifold inlet for the CIMS with two operating modes [30]. In the first mode, gases are directly sampled into a turbulent flow ion-molecule reactor while particles are concurrently collected on a PTFE filter via a separate dedicated port. In the second mode, the filter is automatically moved into a pure N_2 gas stream flowing into the ion-molecule reactor while the N_2 is heated to evaporate the particles via temperature programmed desorption. Analytes are then chemically ionized and extracted into a long ToF-MS, achieving sensitivities below 10^6 cm^{-3} on a 1-minute average with very high mass resolution (up to 14,000) [31]. This technique enhances our ability to explore the partitioning between the gas and particle phases driving the aerosol behavior. In addition, during CLOUD-11, H_2SO_4 and oxidized organic vapor concentrations were routinely measured with a nitrate-ion based Chemical Ionization Atmospheric Pressure interface Time-of-Flight mass spectrometer (nitrate-CI-APi-ToF) [7]. Calibration and corrections of sulfuric acid are similar to our previous work [32].

Particle size distribution. Particle size distributions were measured by several sizing instruments optimized for different size ranges. Particles in the size range between 1.8−8 nm were measured by the so-called DMA-train [9], and the corresponding growth-rate calculations were performed with the appearance time method, which is effective in chamber experiments where a clear front of a growing particle population can be identified during most nucleation and growth events. Larger particles between 5−65 nm were measured with a scanning mobility particle sizer (TSI nano-SMPS, model 3982).

Volatility measurements. Organic compounds with different vapor pressures have distinct and reproducible thermograms during thermal desorption, and the maximum desorption temperature (T_{max}) correlates with the vaporization enthalpy and thus is a function of the vapor pressure. We calibrated the thermal-desorption volatility measurements using a suite of standards with known vapor pressures [30,33]. Briefly, we dissolved a set of organic acids in isopropanol at low concentrations and manually deposited them on the FIGAERO filter with a microliter syringe. We then held the mixture of acids at room temperature for 1 minute to allow the solvent to evaporate before following the same thermal-desorption protocol used for chamber experiments. We then established a thermal-desorption volatility calibration curve by

correlating $1/T_{max}$ (1/K) with the sub-cooled liquid vapor pressure of each calibrant (Figure S1). One potential source of uncertainty is that dimers may decompose to monomers when heated, appearing as doublet-peaks in the thermogram [34]. However, in this study, as dimer formation is suppressed by NO_x, thermal decomposition of dimers did not affect the T_{max} of monomers.

RESULTS AND DISCUSSION

Direct measurement of particle-phase volatility. In the experiments described above we directly measured the volatility of particle-phase products formed from photo-oxidation of representative aromatic precursors (toluene and naphthalene) via their thermal-desorption profile using an I^- FIGAERO-CIMS (see MATERIALS AND METHODS). In Figure 1, we display the results in the two-dimensional volatility basis set (2D-VBS) [35], with volatility (saturation concentration, C^*, in μg m^{-3}) on the *x*-axis and the oxygenation (oxygen to carbon ratio, O:C) on the *y*-axis. We choose C^* and O:C as two complementary coordinates because they explicitly track properties that we can observe in experiments and in the atmosphere, and that we need to know to accurately model organic aerosol behavior.

In Figure 1A, we show monomers (crosses) and dimers (dots) derived from photo-oxidation of toluene (blue symbols) and naphthalene (gray symbols) with NO_x present. Almost all of the naphthalene-derived dimers appear in the ULVOC range [36], but the toluene-derived dimers span the LVOC and ELVOC ranges. The measured monomers mostly appear in the LVOC range, with a minority of the naphthalene-derived monomers being ELVOCs. Red dashed lines are carbon numbers isopleths (C_6, C_{11} and C_{19}); these are derived from the original 2D-VBS volatility parameterization, developed before the role of autoxidation in atmospheric chemistry was appreciated [37], which assumed that a 50-50 mixture of –OH and =O functionalities dominated the oxidized organics [35]. These contours coincide well with our measured volatilities from aromatic precursors. Toluene-derived monomers and naphthalene-derived dimers fall along the C_6 and C_{19} isopleths, respectively, and toluene-derived dimers and naphthalene-derived monomers overlap along the C_{11} isopleths. Measured monomers are slightly more spread than dimers, potentially due to thermal decomposition or dehydration.

Similar to our aromatic oxidation experiments, in Figure 1B, we present monomers (green

crosses) and dimers (green dots) from α-pinene ozonolysis in the presence of NO_x. The carbon number isopleths (C_{10} and C_{19}, black dashed lines) are calculated using a revised VBS parameterization to reflect the contribution of autoxidation and subsequent –OOH functionality formation to initial particle growth [9]. The measured dimers align with the C_{19} isopleth with great fidelity, though monomers are systematically but only slightly less volatile than the C_{10} isopleth. In this case, NO terminates the nascent peroxy radicals, suppresses autoxidation, and thus reduces the product oxygen numbers. As a result, the overall product volatility distribution is shifted towards the volatile end of the distribution compared to NO_x-free products (the oxygens on the $–NO_2$ moiety are not counted in O:C). Nevertheless, the products remain well described by the modified C^* vs O:C isopleths, with much higher volatility than the "traditional" VBS.

Compared with the α-pinene-derived oxidation products (C_{10}), toluene-derived products reach a similar volatility and O:C range with a C_7 backbone. More interestingly, naphthalene-derived oxidation products are much less volatile than α-pinene-derived products, though both start with a C_{10} backbone. The general volatility difference between dimers from these two precursors is ~5 orders of magnitude, as illustrated in Figure 1C and Figure S2. Aromatic oxidation appears to use oxygen atoms much more efficiently to form low-volatility products, consistent with the observation that bulk aromatic aerosols have a larger volume fraction remaining (VFR) after heating than biogenic aerosols [38].

In Figure S3, we show the measured volatilities of aromatic- and α-pinene-derived oxidation products versus corresponding volatilities estimated using the VBS parametrizations in Donahue *et al.* [35] and Stolzenburg *et al.* [9], respectively. Here, we choose organic compounds with six or more oxygen atoms to minimize the uncertainty of thermal decomposition in the FIGAERO. A good correlation (r^2 of 0.77) verifies the consistency between direct FIGAERO volatility measurements and VBS parameterizations.

Correlation between volatility and growth rate. Because the volatility of photo-oxidation products can vary by more than 10 orders of magnitude, it is convenient to simplify consideration of gas-particle partitioning by grouping compounds together within the VBS. In Figure 2A and B we show the binned volatility distribution of all organic particle-phase compounds observed with our FIGAERO-CIMS for the two representative aromatic

hydrocarbons. The volatility of toluene-derived oxidation products (Figure 2A) ranges from 10^{-9} to 10^{-2} μg m^{-3} with one mode at 10^{-4} and the other at 10^{-8} μg m^{-3}. Naphthalene oxidation products are even less volatile (Figure 2B), with saturation concentrations ranging from 10^{-12} to 10^{-2} μg m^{-3}. We divide the measured oxidation products into four groups: organonitrate monomers (light blue), pure organic monomers (light green), organonitrate dimers (navy blue) and pure organic dimers (dark green). For both of the monomers and dimers, organonitrates tend to be more volatile than non-nitrate products. This is again consistent with the NO_x effect on monoterpene oxidation and can also be explained either by the termination of nascent peroxy radicals or by reduced product reactivity with OH radicals and thus less secondary oxidation.

The measured volatility distributions are consistent with the 3−8 nm growth-rate measurements, where in Figure 2C we compare observed growth rates with gas-phase oxidation products measured with a nitrate-CI-APi-TOF [13]. With most of the products in the LVOC range, toluene-derived oxidation products are somewhat less efficient than H_2SO_4 at driving growth. Naphthalene oxidation, on the other hand, produces a large amount of ULVOCs and ELVOCs, which are relatively more efficient at driving growth. The consistency between volatility and growth-rate measurements makes sense since all the species that can be measured in the particle phase must contribute to the particle growth, thus their volatilities can be taken as the criteria of growing particles and be used by VBS microphysical growth models.

The relative contribution of different precursors to new-particle formation depends on the volatility distribution of the products as well as the relative concentrations of the precursors. In polluted urban atmospheres, the concentration of aromatic hydrocarbons will exceed that of monoterpenes to be the dominant VOC precursors. Further, NO_x will substantially suppress the formation of monoterpene-derived ELVOCs, making the role of aromatic-derived oxidation products even more important. It is thus essential to add the volatility distribution of aromatic-derived oxidation products into particle-growth models and to assess the growth rates observed in urban areas.

Influence of functionality on volatility. Volatility is affected by both the molar weight and polarity of a molecule. Therefore, molecular structure and functionality matter. As a hydrocarbon chain gets larger, the increase in number of electrons increases the temporary

dipoles causing stronger van der Waals' forces and thus reducing the volatility. According to the SIMPOL model [39], each carbon atom lowers log C^* by 0.44. However, toluene has fewer carbon atoms than α-pinene, yet forms oxidation products with a comparable volatility distribution (see Figure 1). This is not due directly to aromaticity; each aromatic ring only lowers log C^* by 0.68. Even more notably, the 4 to 5 decades general difference between naphthalene-derived and α-pinene-derived oxidation products cannot be explained by different structures of their carbon backbones. This leaves functionality as the driving factor; the identity of the added functional groups plays a major role in volatility. Addition of one oxygen-containing functional group, in general, has a greater effect on volatility than a one-carbon increase in the size of the carbon skeleton, but the exact nature of the functional group is very important. Polar functional groups promote dipole-dipole interactions and thus will result in a larger decrease in volatility (e.g. each aldehyde group reduces log C^* by 1.35, and ketone group by 0.94). Functional groups that enable hydrogen bonding between molecules result in an even larger decrease in volatility (e.g. each hydroxyl group reduces log C^* by 2.23, hydroperoxide group by 2.48 (1.24 per oxygen), and carboxylic acid group by 3.58 (1.79 per oxygen)) [39].

We investigate the influence of oxygen-containing functional groups on volatility of aromatic- and α-pinene-derived oxidation products by performing a parameterization using FIGAERO volatility data. This parameterization is based on a simple, three-parameter group-contribution expression:

$$\log_{10} C^*_{300} = \left(n_C^0 - n_C\right) b_C - n_O b_O \quad (1)$$

where C^*_{300} (at 300 K) is calculated from SIMPOL or directly measured by FIGAERO; $n_C^0 = 25$ is the carbon number n_C with $C^O = 1\ \mu g\ m^{-3}$ for pure hydrocarbons; $b_C = 0.48$ is the average effect of each added carbon on $\log_{10} C^*$; b_O indicates the average effect of each added oxygen on $\log_{10} C^*$ [35]. Note that a nitrate group ($-ONO_2$) typically reduces vapor pressure by about 2.5 orders of magnitude, so we replace any $-ONO_2$ group by –OH for simplicity.

Here, instead of using this parameterization to calculate volatility, we fit the parameter b_O using volatility measured with FIGAERO thermal desorption. We performed the parameterization for products from α-pinene ozonolysis, toluene photo-oxidation and

naphthalene photo-oxidation, all with NO_x (green, blue and gray symbols in Figure 1, respectively).

The fitted b_O value for α-pinene-derived oxidation products with NO_x present is 0.91. This is consistent with hydroperoxide, ketone and aldehyde functionalities (roughly 1 decade per oxygen) proposed in Tröstl *et al.* [1]. To the extent that these simple group-contribution values can be extrapolated to multifunctional compounds, this appears to be general within the confines of this dataset; it certainly applies at the low-O:C limit, and it is reasonable for bi-functional compounds (e.g. diacids [40]). Many of the low-volatility particle-phase products from monoterpene oxidation may thus be first-generation autoxidation products containing multiple –OOH functional groups.

The fitted b_O values for toluene-derived and naphthalene-derived oxidation products, on the other hand, are 1.55 and 1.72, respectively, suggesting more hydroxyl or carboxylic acid functionality in aromatic-derived products. Oxygen-containing groups are very likely the key to the systematic volatility difference between aromatic and monoterpene oxidation systems, so we investigate the chemical mechanism in the next section in order to further understand the formation of these functional groups in aromatic oxidation systems.

Formation of oxidation products of aromatic hydrocarbons. In this section, we use toluene as the example to consider the chemical mechanism of aromatic oxidation. With this proposed mechanism, we are able to address the volatility distributions arising from aromatics and evaluate the contribution of aromatic-derived oxidation products to new-particle formation.

The detailed chemical mechanism of toluene oxidation in the atmosphere remains uncertain. Wu *et al*. [41] suggested that over 75% bicyclic peroxy radicals (BPRs) are formed after the first OH oxidation of toluene based on a modified MCM mechanism. Wang *et al*. [42], combining quantum calculations and flow-tube experiments, proposed that unimolecular H-migration followed by O_2-addition, a so-called autoxidation step, can take place in BPRs, which are important intermediates of the OH-initiated oxidation of alkyl benzenes [43]. On the other hand, Ji *et al*. [44] reported that cresols are much more stable than their corresponding peroxy radicals [45], and, for the most favorable OH (ortho) addition, the pathway of H abstraction by O_2 to form the cresol is dominant and O_2 addition to form the peroxy radical is negligible. Other comprehensive studies [46,47] identified ring-retaining products from cresol

oxidation and quantified both the yields of dihydroxy toluene and trihydroxy toluene being ~ 0.7, which supported the results from Ji *et al.* [44].

These seemingly disparate findings may not be contradictory, since product formation pathways and their yields depend strongly on experimental conditions. In the case of toluene oxidation, the concentrations of OH radicals and O_2 control the relative importance of OH oxidation and autoxidation, respectively. Wang *et al.* [42] worked with [OH] of (2.4−53) × 10^4 cm^{-3} in their experiments, which is one to two orders of magnitude lower than in ambient conditions. The predominance of BPRs observed in their experiments could be due to suppressed OH oxidation. However, in Ji's experiments [44], the concentration of O_2 was 10^{15} cm^{-3}, roughly 5000 times lower than in the atmospheric boundary layer ($[O_2] = 5 \times 10^{18}$ cm^{-3}), which could substantially suppress the formation of peroxy radicals.

In the CLOUD experiments, we set the experimental conditions as close as possible to ambient conditions in order to acquire insights into the mechanisms that are atmospherically relevant. We used [OH] of ~ 10^6 cm^{-3} and the [NO_x] of ~ 15 ppbv for the experiments in this study. Also, the iodide reagent ion in our FIGAERO is sensitive to a wide range of species, enabling us to observe oxygenated organics with oxygen numbers down to one or two with good fidelity [48]. Under these conditions, we observed products from both categories. In Figure 3 we show a mass defect plot of monomers from toluene oxidation measured in the gas phase. The *x*-axis is the exact mass of the products and the *y*-axis is the mass defect. Each straight line represents a homologous sequence of compounds with the same number of carbon, hydrogen, and nitrogen atoms, but a different number of oxygen atoms. Notably, there are two main categories of products: $C_7H_8O_{2\text{-}6}$, which likely preserves the aromaticity, and $C_7H_{10}O_{4\text{-}8}$, which breaks the aromatic ring. These aromatic ring-retaining and aromatic ring-opening products are associated with organonitrates, $C_7H_7NO_{3\text{-}7}$ and $C_7H_9NO_{5\text{-}10}$, respectively, via the termination of the corresponding peroxy radicals by NO.

The detailed toluene oxidation mechanism is instructive (see Figure 4). Briefly, the rate of OH addition to an aromatic ring is proportional to the electrophilic nature of the substituents around the ring. Being electrophilic, the added OH groups in turn facilitate further addition reactions by increasing the electron density on the ring through a resonance donating effect and thus activating the aromatic ring. Following the ring-retaining pathway for toluene, OH radical

addition to the aromatic ring can occur multiple times to form cresol, dihydroxy-, trihydroxy- and even multi-OH substituted-toluene (i.e. $C_7H_8O_{2\text{-}6,}$). The fact that we did not observe a significant amount of cresol could be due to its relatively slow production and fast consumption, which yields a low steady-state vapor concentration. This is consistent with the large signal we observed for $C_7H_7NO_3$, most likely hydroxy nitrotoluene, formed from the reaction of methyl phenoxy radicals with NO_2 or the reaction of cresol with NO_3 radicals [47].

Along the ring-opening pathway, peroxy radical production is followed by formation of bicyclic peroxides (i.e. $C_7H_{10}O_{4\text{-}8}$), which generates oxidation products with oxygen numbers of 8 or more. A succession of unimolecular H-migration reactions followed by O_2 addition (so-called autoxidation) can take place rapidly in bicyclic peroxy radicals (BPRs), which are important intermediates of the OH-initiated oxidation of aromatic compounds, possibly leading to the formation of highly oxygenated organic molecules (HOMs). However, with NO_x present in the chamber, peroxy-radical autoxidation is substantially suppressed, and we observed low HOM concentrations. Further, we also observed various decomposition products (C_5 and C_6) attributable to the bicyclic intermediate pathway. Although we distinguish the OH oxidation pathway from the autoxidation pathway, product formation in reality does not follow only one pathway. OH oxidation and autoxidation both can occur; it is their branching ratio under different conditions that matters.

Our purpose here is not to comprehensively define the detailed mechanism, but rather to demonstrate that aromatics are qualitatively different from monoterpenes in terms of the chemical mechanisms of photo-oxidation leading to new-particle formation and particle growth. From the proposed mechanism and from our FIGAERO observations, we conclude that rapid progression through multiple generations of OH oxidation is more pronounced in toluene and naphthalene than that in α-pinene, resulting in not only more oxidation but crucially also functional groups with much lower volatility per added oxygen atom, such as hydroxyl and carboxylic acids. For example, our proposed $C_7H_xO_{5\text{-}7}$ products from toluene contain up to 4 hydroxyl groups, while $C_{10}H_xO_{5\text{-}7}$, from α-pinene proposed in Tröstl *et al.* [1], only contain at most 1 hydroxyl group. Since hydroxyl groups have a much stronger effect per oxygen on volatility (stronger by about 1 decade per oxygen than –OOH), the larger number of hydroxyl groups accounts for the 4 to 5 decades difference in volatility between aromatic- and α-pinene-

366 derived oxidation products we observe in Figure 1.

367 These findings are consistent with findings for bulk SOA formation from monoterpenes
368 and aromatics [49]. Specifically, with monoterpenes (especially for ozonolysis), SOA mass yields
369 can be reasonably described by first-generation products and a relatively stable product
370 distribution following the initial ozonolysis. For toluene photo-oxidation, on the other hand,
371 models of SOA formation in chambers must consider multiple generations of OH reaction
372 because the products become progressively more reactive with OH as the generation number
373 increases. To account for these differences, two different 2D-VBS representations of SOA
374 formation and aging have been developed for chemical transport models [50]. Our findings
375 confirm this. The volatility parameter $b_O \sim 1.6$ we derive for aromatic oxidation is consistent
376 with the original 2D-VBS parameterization representing aging and oxygenation of organic
377 products principally with an equal mixture of =O and –OH functional groups (and –C(O)OH).
378 This is a "traditional aging" scenario. On the other hand, the volatility parameter $b_O \sim 0.9$ we
379 derive for α-pinene oxidation is consistent with the modified parameterizations more recently
380 employed to represent prompt formation of multiple –OOH functional groups. This is an
381 "autoxidation" scenario.

382 It is important to note that these scenarios are not mutually exclusive. As we discussed,
383 autoxidation does occur in the aromatic systems, and most of the first-generation monoterpene
384 products are not HOMs that have undergone autoxidation. All of these (mostly gas-phase)
385 products will almost certainly undergo further oxidation in the atmosphere, often on short
386 timescales [51], and some of these second and later generation products will also undergo
387 autoxidation, as previous CLOUD experiments have shown for the first-generation
388 monoterpene product pinanediol [16,52].

389 Photo-oxidation of aromatic compounds (toluene and naphthalene) efficiently produces
390 low-volatility products that participate in new-particle formation and growth under conditions
391 typical of polluted urban settings. Here we have measured the composition of newly formed
392 particles with a FIGAERO-CIMS and directly constrained the volatility distribution of the
393 oxidation products that drive new-particle formation and growth. We find that oxidation of
394 toluene and naphthalene by OH radicals makes efficient use of added oxygen to form low-
395 volatility products, with much larger reductions in volatility per added oxygen atom than

corresponding α-pinene systems. This is consistent with known differences in the oxidation mechanisms of aromatics and monoterpenes. Particle formation and growth in urban airmasses may thus be strongly influenced by aromatic precursors.

ASSOCIATED CONTENT

Supporting Information

The Supporting Information is available free of charge on the ACS Publications website. This file includes correlation of inverse maximum desorption temperature ($1/T_{max}$) and the saturation concentration (log C^*) (Figure S1); example of thermograms (Figure S2); measured and predicted volatility (Figure S3).

AUTHOR INFORMATION

Corresponding Author

*Neil M. Donahue (E-mail: nmd@andrew.cmu.edu).

Author Contributions

M. W., D. C., M. X., J. K., D. R. W., U. B., J. Dommen, I. E.-H., and N. M. D. designed research; M. W., D. C., M. X., Q. Y., D. S., V. H., P. Y., A. L. V., R. L. M., A. A., A. B., B. B., S. B., L. D., A. D., J. Duplissy, H. F., O. G., X. H., C. R. H., C. K., A. K., K. L., F. L., U. M., T. P., V. P., L. L. J. Q., M. R., M. S., C. T., A. T., A. C. W., L. W., J. K., J. Dommen, and I. E.-H. performed research; M. W., M. X., D. S., and N. M. D. contributed new reagents/analytic tools; M. W., M. X., D. S., P. Y., and M. S. analyzed data; and M. W., D. C., M. X., A. L. V., U. M., J. K., U. B., J. Dommen, I. E.-H., and N. M. D. wrote the paper.

Notes

The authors declare no competing financial interest.

ACKNOWLEDGEMENT

We thank the European Organization for Nuclear Research (CERN) for supporting CLOUD with important technical and financial resources and for providing a particle beam from the CERN Proton Synchrotron. This research has received funding from the U.S. National Science Foundation under grants AGS-1447056, AGS-1439551, AGS-1649147, AGS-1602086, and

AGS-1801897; the German Federal Ministry of Education and Research (No. 01LK1601A); ERC-Consolidator Grant NANODYNAMITE 616075; Horizon 2020 Marie Skłodowska-Curie Grant 656994 ("Nano-CAVa"); ERC Advanced "ATM-GP" grant No. 227463; the Presidium of the Russian Academy of Sciences, the Program "High energy physics and neutrino astrophysics" 2015; the Swiss National Science Foundation Projects 200020_152907, 20FI20_159851, 200021_169090, 200020_172602 and 20FI20_172622. The FIGAERO-CIMS was supported by an MRI grant for the U.S. NSF AGS-1531284 as well as the Wallace Research Foundation. O.G. thanks Doctoral Programme in Atmospheric Sciences at the University of Helsinki for financial support.

REFERENCES

(1) Tröstl, J.; Chuang, W. K.; Gordon, H.; Heinritzi, M.; Yan, C.; Molteni, U.; Ahlm, L.; Frege, C.; Bianchi, F.; Wagner, R.; Simon, M.; Lehtipalo, K.; Williamson, C.; Craven, J. S.; Duplissy, J.; Adamov, A.; Almeida, J.; Bernhammer, A. K.; Breitenlechner, M.; Brilke, S.; Dias, A.; Ehrhart, S.; Flagan, R. C.; Franchin, A.; Fuchs, C.; Guida, R.; Gysel, M.; Hansel, A.; Hoyle, C. R.; Jokinen, T.; Junninen, H.; Kangasluoma, J.; Keskinen, H.; Kim, J.; Krapf, M.; Kürten, A.; Laaksonen, A.; Lawler, M.; Leiminger, M.; Mathot, S.; Möhler, O.; Nieminen, T.; Onnela, A.; Petäjä, T.; Piel, F. M.; Miettinen, P.; Rissanen, M. P.; Rondo, L.; Sarnela, N.; Schobesberger, S.; Sengupta, K.; Sipilä, M.; Smith, J. N.; Steiner, G.; Tomè, A.; Virtanen, A.; Wagner, A. C.; Weingartner, E.; Wimmer, D.; Winkler, P. M.; Ye, P.; Carslaw, K. S.; Curtius, J.; Dommen, J.; Kirkby, J.; Kulmala, M.; Riipinen, I.; Worsnop, D. R.; Donahue, N. M.; Baltensperger, U. The Role of Low-Volatility Organic Compounds in Initial Particle Growth in the Atmosphere. *Nature* **2016**, *533* (7604), 527–531. https://doi.org/10.1038/nature18271.

(2) Apte, J. S.; Marshall, J. D.; Cohen, A. J.; Brauer, M. Addressing Global Mortality from Ambient PM2.5. *Env. Sci Technol* **2015**, *49* (13), 8057–8066. https://doi.org/10.1021/acs.est.5b01236.

(3) Lelieveld, J.; Evans, J. S.; Fnais, M.; Giannadaki, D.; Pozzer, A. The Contribution of Outdoor Air Pollution Sources to Premature Mortality on a Global Scale. *Nature* **2015**, *525* (7569), 367–371. https://doi.org/10.1038/nature15371.

(4) Riipinen, I.; Yli-Juuti, T.; Pierce, J. R.; Petaja, T.; Worsnop, D. R.; Kulmala, M.; Donahue, N. M.; Petäjä, T.; Worsnop, D. R.; Kulmala, M.; Donahue, N. M. The Contribution of Organics to Atmospheric Nanoparticle Growth. *Nat. Geosci.* **2012**, *5* (7), 453–458. https://doi.org/10.1038/ngeo1499.

(5) Anttila, T.; Kerminen, V.-M. M.; Lehtinen, K. E. J. J. Parameterizing the Formation Rate of New Particles: The Effect of Nuclei Self-Coagulation. *J. Aerosol Sci.* **2010**, *41* (7), 621–636. https://doi.org/10.1016/j.jaerosci.2010.04.008.

(6) Solomon, S.; Manning, M.; Marquis, M.; Qin, D.; others. *Climate Change 2007-the Physical Science Basis: Working Group I Contribution to the Fourth Assessment Report of the IPCC*; Cambridge university press, 2007; Vol. 4.

(7) Kirkby, J.; Duplissy, J.; Sengupta, K.; Frege, C.; Gordon, H.; Williamson, C.; Heinritzi, M.; Simon, M.; Yan, C.; Almeida, J.; Trostl, J.; Nieminen, T.; Ortega, I. K.; Wagner, R.; Adamov, A.; Amorim, A.; Bernhammer, A. K.; Bianchi, F.; Breitenlechner, M.; Brilke, S.; Chen, X. M.; Craven, J.; Dias, A.; Ehrhart, S.; Flagan, R. C.; Franchin, A.; Fuchs, C.; Guida, R.; Hakala, J.; Hoyle, C. R.; Jokinen, T.; Junninen, H.; Kangasluoma, J.; Kim, J.; Krapf, M.; Kurten, A.; Laaksonen, A.; Lehtipalo, K.; Makhmutov, V.; Mathot, S.; Molteni, U.; Onnela, A.; Perakyla, O.; Piel, F.; Petaja, T.; Praplan, A. P.; Pringle, K.; Rap, A.; Richards, N. A. D. D.; Riipinen, I.; Rissanen, M. P.; Rondo, L.; Sarnela, N.; Schobesberger, S.; Scott, C. E.; Seinfeld, J. H.; Sipila, M.; Steiner, G.; Stozhkov, Y.; Stratmann, F.; Tome, A.; Virtanen, A.; Vogel, A. L.; Wagner, A. C.; Wagner, P. E.; Weingartner, E.; Wimmer, D.; Winkler, P. M.; Ye, P. L.; Zhang, X.; Hansel, A.; Dommen, J.; Donahue, N. M.; Worsnop, D. R.; Baltensperger, U.; Kulmala, M.; Carslaw, K. S.; Curtius, J.; Tomé, A.; Virtanen, A.; Vogel, A. L.; Wagner, A. C.; Wagner, P. E.; Weingartner, E.; Wimmer, D.; Winkler, P. M.; Ye, P. L.; Zhang, X.; Hansel, A.; Dommen, J.; Donahue, N. M.; Worsnop, D. R.; Baltensperger, U.; Kulmala, M.; Carslaw, K. S.; Curtius, J. Ion-Induced Nucleation of Pure Biogenic Particles. *Nature* **2016**, *533* (7604), 521–526. https://doi.org/10.1038/nature17953.

(8) Lehtipalo, K.; Yan, C.; Dada, L.; Bianchi, F.; Xiao, M.; Wagner, R.; Stolzenburg, D.; Ahonen, L. R.; Amorim, A.; Baccarini, A.; Bauer, P. S.; Baumgartner, B.; Bergen, A.; Bernhammer, A.-K.; Breitenlechner, M.; Brilke, S.; Buchholz, A.; Mazon, S. B.; Chen, D.; Chen, X.; Dias, A.; Dommen, J.; Draper, D. C.; Duplissy, J.; Ehn, M.; Finkenzeller, H.; Fischer, L.; Frege, C.; Fuchs, C.; Garmash, O.; Gordon, H.; Hakala, J.; He, X.; Heikkinen, L.; Heinritzi, M.; Helm, J. C.; Hofbauer, V.; Hoyle, C. R.; Jokinen, T.; Kangasluoma, J.; Kerminen, V.-M.; Kim, C.; Kirkby, J.; Kontkanen, J.; Kürten, A.; Lawler, M. J.; Mai, H.; Mathot, S.; Mauldin, R. L.; Molteni, U.; Nichman, L.; Nie, W.; Nieminen, T.; Ojdanic, A.; Onnela, A.; Passananti, M.; Petäjä, T.; Piel, F.; Pospisilova, V.; Quéléver, L. L. J.; Rissanen, M. P.; Rose, C.; Sarnela, N.; Schallhart, S.; Schuchmann, S.; Sengupta, K.; Simon, M.; Sipilä, M.; Tauber, C.; Tomé, A.; Tröstl, J.; Väisänen, O.; Vogel, A. L.; Volkamer, R.; Wagner, A. C.; Wang, M.; Weitz, L.;

Wimmer, D.; Ye, P.; Ylisirniö, A.; Zha, Q.; Carslaw, K. S.; Curtius, J.; Donahue, N. M.; Flagan, R. C.; Hansel, A.; Riipinen, I.; Virtanen, A.; Winkler, P. M.; Baltensperger, U.; Kulmala, M.; Worsnop, D. R. Multicomponent New Particle Formation from Sulfuric Acid, Ammonia, and Biogenic Vapors. *Sci. Adv.* **2018**, *4* (12), eaau5363. https://doi.org/10.1126/sciadv.aau5363.

(9) Stolzenburg, D.; Fischer, L.; Vogel, A. L.; Heinritzi, M.; Schervish, M.; Simon, M.; Wagner, A. C.; Dada, L.; Ahonen, L. R.; Amorim, A.; Baccarini, A.; Bauer, P. S.; Baumgartner, B.; Bergen, A.; Bianchi, F.; Breitenlechner, M.; Brilke, S.; Buenrostro Mazon, S.; Chen, D.; Dias, A.; Draper, D. C.; Duplissy, J.; El Haddad, I.; Finkenzeller, H.; Frege, C.; Fuchs, C.; Garmash, O.; Gordon, H.; He, X.; Helm, J.; Hofbauer, V.; Hoyle, C. R.; Kim, C.; Kirkby, J.; Kontkanen, J.; Kürten, A.; Lampilahti, J.; Lawler, M.; Lehtipalo, K.; Leiminger, M.; Mai, H.; Mathot, S.; Mentler, B.; Molteni, U.; Nie, W.; Nieminen, T.; Nowak, J. B.; Ojdanic, A.; Onnela, A.; Passananti, M.; Petäjä, T.; Quéléver, L. L. J.; Rissanen, M. P.; Sarnela, N.; Schallhart, S.; Tauber, C.; Tomé, A.; Wagner, R.; Wang, M.; Weitz, L.; Wimmer, D.; Xiao, M.; Yan, C.; Ye, P.; Zha, Q.; Baltensperger, U.; Curtius, J.; Dommen, J.; Flagan, R. C.; Kulmala, M.; Smith, J. N.; Worsnop, D. R.; Hansel, A.; Donahue, N. M.; Winkler, P. M. Rapid Growth of Organic Aerosol Nanoparticles over a Wide Tropospheric Temperature Range. *Proc. Natl. Acad. Sci.* **2018**, *115* (37), 9122–9127. https://doi.org/10.1073/pnas.1807604115.

(10) Donahue, N. M.; Ortega, I. K.; Chuang, W.; Riipinen, I.; Riccobono, F.; Schobesberger, S.; Dommen, J.; Baltensperger, U.; Kulmala, M.; Worsnop, D. R.; Vehkamaki, H. How Do Organic Vapors Contribute to New-Particle Formation? *Faraday Discuss.* **2013**, *165*, 91–104. https://doi.org/10.1039/c3fd00046j.

(11) Jokinen, T.; Sipila, M.; Richters, S.; Kerminen, V. M.; Paasonen, P.; Stratmann, F.; Worsnop, D.; Kulmala, M.; Ehn, M.; Herrmann, H.; Berndt, T. Rapid Autoxidation Forms Highly Oxidized RO2 Radicals in the Atmosphere. *Angew. Chemie-International Ed.* **2014**, *53*, 14596–14600. https://doi.org/10.1002/anie.201408566.

(12) Ehn, M.; Thornton, J. A.; Kleist, E.; Sipila, M.; Junninen, H.; Pullinen, I.; Springer, M.; Rubach, F.; Tillmann, R.; Lee, B.; Lopez-Hilfiker, F.; Andres, S.; Acir, I. H.; Rissanen, M.; Jokinen, T.; Schobesberger, S.; Kangasluoma, J.; Kontkanen, J.; Nieminen, T.; Kurten, T.; Nielsen, L. B.; Jorgensen, S.; Kjaergaard, H. G.; Canagaratna, M.; Maso, M. D.; Berndt, T.; Petaja, T.; Wahner, A.; Kerminen, V. M.; Kulmala, M.; Worsnop, D. R.; Wildt, J.; Mentel, T. F.; Dal Maso, M.; Berndt, T.; Petaja, T.; Wahner, A.; Kerminen, V. M.; Kulmala, M.; Worsnop, D. R.; Wildt, J.; Mentel, T. F. A Large Source of Low-Volatility Secondary Organic Aerosol. *Nature* **2014**, *506* (7489), 476–479.

https://doi.org/10.1038/nature13032.

(13) Yan, C.; Nie, W.; Vogel, A. L.; Dada, L.; Lehtipalo, K.; Stolzenburg, D.; Wagner, R.; Rissanen, M. P.; Xiao, M.; Ahonen, L.; Fischer, L.; Rose, C.; Bianchi, F.; Gordon, H.; Simon, M.; Heinritzi, M.; Garmash, O.; Roldin, P.; Dias, A.; Ye, P.; Hofbauer, V.; Amorim, A.; Bauer, P. S.; Bergen, A.; Bernhammer, A.-K.; Breitenlechner, M.; Brilke, S.; Buchholz, A.; Mazon, S. B.; Canagaratna, M. R.; Chen, X.; Ding, A.; Dommen, J.; Draper, D. C.; Duplissy, J.; Frege, C.; Heyn, C.; Guida, R.; Hakala, J.; Heikkinen, L.; Hoyle, C. R.; Jokinen, T.; Kangasluoma, J.; Kirkby, J.; Kontkanen, J.; Kürten, A.; Lawler, M. J.; Mai, H.; Mathot, S.; Mauldin, R. L.; Molteni, U.; Nichman, L.; Nieminen, T.; Nowak, J.; Ojdanic, A.; Onnela, A.; Pajunoja, A.; Petäjä, T.; Piel, F.; Quéléver, L. L. J.; Sarnela, N.; Schallhart, S.; Sengupta, K.; Sipilä, M.; Tomé, A.; Tröstl, J.; Väisänen, O.; Wagner, A. C.; Ylisirniö, A.; Zha, Q.; Baltensperger, U.; Carslaw, K. S.; Curtius, J.; Flagan, R. C.; Hansel, A.; Riipinen, I.; Smith, J. N.; Virtanen, A.; Winkler, P. M.; Donahue, N. M.; Kerminen, V.-M.; Kulmala, M.; Ehn, M.; Worsnop, D. R. Size-Dependent Influence of NOx on the Growth Rates of Organic Aerosol Particles. *Sci. Adv.* **2020**, *6* (22). https://doi.org/10.1126/sciadv.aay4945.

(14) Rissanen, M. P.; Kurtén, T.; Sipilä, M.; Thornton, J. A.; Kangasluoma, J.; Sarnela, N.; Junninen, H.; Jørgensen, S.; Schallhart, S.; Kajos, M. K.; Taipale, R.; Springer, M.; Mentel, T. F.; Ruuskanen, T.; Petäjä, T.; Worsnop, D. R.; Kjaergaard, H. G.; Ehn, M.; Kurtén, T.; Sipilä, M.; Thornton, J. A.; Kangasluoma, J.; Sarnela, N.; Junninen, H.; Jørgensen, S.; Schallhart, S.; Kajos, M. K.; Kurten, T.; Sipila, M.; Thornton, J. A.; Kangasluoma, J.; Sarnela, N.; Junninen, H.; Jorgensen, S.; Schallhart, S.; Kajos, M. K.; Taipale, R.; Springer, M.; Mentel, T. F.; Ruuskanen, T.; Petaja, T.; Worsnop, D. R.; Kjaergaard, H. G.; Ehn, M. The Formation of Highly Oxidized Multifunctional Products in the Ozonolysis of Cyclohexene. *J. Am. Chem. Soc.* **2014**, *136*, 15596–15606. https://doi.org/10.1021/ja507146s.

(15) Donahue, N. M.; Henry, K. M.; Mentel, T. F.; Kiendler-Scharr, A.; Spindler, C.; Bohn, B.; Brauers, T.; Dorn, H. P.; Fuchs, H.; Tillmann, R.; Wahner, A.; Saathoff, H.; Naumann, K.-H. H. K. H.; Möhler, O.; Leisner, T.; Müller, L.; Reinnig, M.-C. C. M. C.; Hoffmann, T.; Salo, K.; Hallquist, M.; Frosch, M.; Bilde, M.; Tritscher, T.; Barmet, P.; Praplan, A. P.; DeCarlo, P. F.; Dommen, J.; Prévôt, A. S. H.; Baltensperger, U. Aging of Biogenic Secondary Organic Aerosol via Gas-Phase OH Radical Reactions. *Proc. Natl. Acad. Sci.* **2012**, *109* (34), 13503–13508. https://doi.org/10.1073/pnas.1115186109.

(16) Schobesberger, S.; Junninen, H.; Bianchi, F.; Lönn, G.; Ehn, M.; Lehtipalo, K.; Dommen, J.; Ehrhart, S.; Ortega, I. K.; Franchin, A.; Nieminen, T.; Riccobono, F.; Hutterli, M.; Duplissy, J.; Almeida, J.; Amorim, A.; Breitenlechner, M.; Downard, A. J.; Dunne, E. M.; Flagan, R. C.; Kajos, M.; Keskinen, H.; Kirkby,

J.; Kupc, A.; Kürten, A.; Kurtén, T.; Laaksonen, A.; Mathot, S.; Onnela, A.; Praplan, A. P.; Rondo, L.; Santos, F. D.; Schallhart, S.; Schnitzhofer, R.; Sipilä, M.; Tomé, A.; Tsagkogeorgas, G.; Vehkamäki, H.; Wimmer, D.; Baltensperger, U.; Carslaw, K. S.; Curtius, J.; Hansel, A.; Petäjä, T.; Kulmala, M.; Donahue, N. M.; Worsnop, D. R.; Lonn, G.; Ehn, M.; Lehtipalo, K.; Dommen, J.; Ehrhart, S.; Ortega, I. K.; Franchin, A.; Nieminen, T.; Riccobono, F.; Hutterli, M.; Duplissy, J.; Almeida, J.; Amorim, A.; Breitenlechner, M.; Downard, A. J.; Dunne, E. M.; Flagan, R. C.; Kajos, M.; Keskinen, H.; Kirkby, J.; Kupc, A.; Kurten, A.; Kurten, T.; Laaksonen, A.; Mathot, S.; Onnela, A.; Praplan, A. P.; Rondo, L.; Santos, F. D.; Schallhart, S.; Schnitzhofer, R.; Sipila, M.; Tome, A.; Tsagkogeorgas, G.; Vehkamaki, H.; Wimmer, D.; Baltensperger, U.; Carslaw, K. S.; Curtius, J.; Hansel, A.; Petaja, T.; Kulmala, M.; Donahue, N. M.; Worsnop, D. R. Molecular Understanding of Atmospheric Particle Formation from Sulfuric Acid and Large Oxidized Organic Molecules. *Proc. Natl. Acad. Sci.* **2013**, *110* (43), 17223–17228. https://doi.org/10.1073/pnas.1306973110.

(17) Koppmann, R. *Volatile Organic Compounds in the Atmosphere*; Wiley Online Library, 2007.

(18) Cabrera-Perez, D.; Taraborrelli, D.; Sander, R.; Pozzer, A. Global Atmospheric Budget of Simple Monocyclic Aromatic Compounds. *Atmos. Chem. Phys.* **2016**, *16* (11).

(19) Shah, S. D.; Ogunyoku, T. A.; Miller, J. W.; Cocker, D. R. On-Road Emission Rates of PAH and n-Alkane Compounds from Heavy-Duty Diesel Vehicles. *Environ. Sci. Technol.* **2005**, *39* (14), 5276–5284.

(20) Conde, F. J.; Ayala, J. H.; Afonso, A. M.; González, V. Emissions of Polycyclic Aromatic Hydrocarbons from Combustion of Agricultural and Sylvicultural Debris. *Atmos. Environ.* **2005**, *39* (35), 6654–6663.

(21) McDonald, J. D.; Zielinska, B.; Fujita, E. M.; Sagebiel, J. C.; Chow, J. C.; Watson, J. G. Emissions from Charbroiling and Grilling of Chicken and Beef. *J. Air Waste Manage. Assoc.* **2003**, *53* (2), 185–194.

(22) Bloss, C.; Wagner, V.; Jenkin, M. E.; Volkamer, R.; Bloss, W. J.; Lee, J. D.; Heard, D. E.; Wirtz, K.; Martin-Reviejo, M.; Rea, G.; Wenger, J. C.; Pilling, M. J. Development of a Detailed Chemical Mechanism (MCMv3.1) for the Atmospheric Oxidation of Aromatic Hydrocarbons. *Atmos. Chem. Phys.* **2005**, *5*, 641–664. https://doi.org/DOI 10.5194/acp-5-641-2005.

(23) Offenberg, J. H.; Lewis, C. W.; Lewandowski, M.; Jaoui, M.; Kleindienst, T. E.; Edney, E. O. Contributions of Toluene and α-Pinene to SOA Formed in an Irradiated Toluene/α-Pinene/NOx/Air Mixture: Comparison of Results Using 14C Content and SOA Organic Tracer Methods. *Environ. Sci. Technol.* **2007**, *41* (11), 3972–3976. https://doi.org/10.1021/es070089+.

(24) Odum, J. R.; Jungkamp, T. P. W. W.; Griffin, R. J.; Flagan, R. C.; Seinfeld, J. H. The Atmospheric

Aerosol-Forming Potential of Whole Gasoline Vapor. *Science (80-.).* **1997**, *276* (5309), 96–99. https://doi.org/DOI 10.1126/science.276.5309.96.

(25) Forstner, H. J. L.; Flagan, R. C.; Seinfeld, J. H. Secondary Organic Aerosol from the Photooxidation of Aromatic Hydrocarbons: Molecular Composition. *Environ. Sci. Technol.* **1997**, *31* (5), 1345–1358. https://doi.org/10.1021/es9605376.

(26) Molteni, U.; Bianchi, F.; Klein, F.; El Haddad, I.; Frege, C.; Rossi, M. J.; Dommen, J.; Baltensperger, U. Formation of Highly Oxygenated Organic Molecules from Aromatic Compounds. *Atmos. Chem. Phys.* **2018**, *18*, 1909–1921. https://doi.org/10.5194/acp-18-1909-2018.

(27) Garmash, O.; Rissanen, M. P.; Pullinen, I.; Schmitt, S.; Kausiala, O.; Tillmann, R.; Zhao, D.; Percival, C.; Bannan, T. J.; Priestley, M.; Hallquist, A. M.; Kleist, E.; Kiendler-Scharr, A.; Hallquist, M.; Berndt, T.; McFiggans, G.; Wildt, J.; Mentel, T. F.; Ehn, M. Multi-Generation OH Oxidation as a Source for Highly Oxygenated Organic Molecules from Aromatics. *Atmos. Chem. Phys.* **2020**, *20*, 515–537. https://doi.org/10.5194/acp-20-515-2020.

(28) Dias, A.; Ehrhart, S.; Vogel, A.; Mathot, S.; Onnela, A.; Almeida, J.; Kirkby, J.; Williamson, C.; Mumford, S. Temperature Uniformity in the CERN CLOUD Chamber. *Atmos. Meas. Tech.* **2017**, *10*, 5075–5088.

(29) Bertram, T. H.; Kimmel, J. R.; Crisp, T. A.; Ryder, O. S.; Yatavelli, R. L. N.; Thornton, J. A.; Cubison, M. J.; Gonin, M.; Worsnop, D. R. A Field-Deployable, Chemical Ionization Time-of-Flight Mass Spectrometer. *Atmos. Meas. Tech.* **2011**, *4*, 1471–1479. https://doi.org/10.5194/amt-4-1471-2011.

(30) Lopez-Hilfiker, F. D.; Mohr, C.; Ehn, M.; Rubach, F.; Kleist, E.; Wildt, J.; Mentel, T. F.; Lutz, A.; Hallquist, M.; Worsnop, D.; Thornton, J. A. A Novel Method for Online Analysis of Gas and Particle Composition: Description and Evaluation of a Filter Inlet for Gases and AEROsols (FIGAERO). *Atmos. Meas. Tech.* **2014**, *7* (4), 983–1001. https://doi.org/10.5194/amt-7-983-2014.

(31) Junninen, H.; Ehn, M.; Petaja, T.; Luosujarvi, L.; Kotiaho, T.; Kostiainen, R.; Rohner, U.; Gonin, M.; Fuhrer, K.; Kulmala, M.; Worsnop, D. R.; Petäjä, T.; Luosujärvi, L.; Kotiaho, T.; Kostiainen, R.; Rohner, U.; Gonin, M.; Fuhrer, K.; Kulmala, M.; Worsnop, D. R. A High-Resolution Mass Spectrometer to Measure Atmospheric Ion Composition. *Atmos. Meas. Tech.* **2010**, *3* (4), 1039–1053. https://doi.org/10.5194/amt-3-1039-2010.

(32) Kurten, A.; Jokinen, T.; Simon, M.; Sipila, M.; Sarnela, N.; Junninen, H.; Adamov, A.; Almeida, J.; Amorim, A.; Bianchi, F.; Breitenlechner, M.; Dommen, J.; Donahue, N. M.; Duplissy, J.; Ehrhart, S.; Flagan, R. C.; Franchin, A.; Hakala, J.; Hansel, A.; Heinritzi, M.; Hutterli, M.; Kangasluoma, J.; Kirkby,

J.; Laaksonen, A.; Lehtipalo, K.; Leiminger, M.; Makhmutov, V.; Mathot, S.; Onnela, A.; Petaja, T.; Praplan, A. P.; Riccobono, F.; Rissanen, M. P.; Rondo, L.; Schobesberger, S.; Seinfeld, J. H.; Steiner, G.; Tome, A.; Trostl, J.; Winkler, P. M.; Williamson, C.; Wimmer, D.; Ye, P. L.; Baltensperger, U.; Carslaw, K. S.; Kulmala, M.; Worsnop, D. R.; Curtius, J.; Kürten, A.; Jokinen, T.; Simon, M.; Sipilä, M.; Sarnela, N.; Junninen, H.; Adamov, A.; Almeida, J.; Amorim, A.; Bianchi, F.; Breitenlechner, M.; Dommen, J.; Donahue, N. M.; Duplissy, J.; Ehrhart, S.; Flagan, R. C.; Franchin, A.; Hakala, J.; Hansel, A.; Heinritzi, M.; Hutterli, M.; Kangasluoma, J.; Kirkby, J.; Laaksonen, A.; Lehtipalo, K.; Leiminger, M.; Makhmutov, V.; Mathot, S.; Onnela, A.; Petäjä, T.; Praplan, A. P.; Riccobono, F.; Rissanen, M. P.; Rondo, L.; Schobesberger, S.; Seinfeld, J. H.; Steiner, G.; Tomé, A.; Tröstl, J.; Winkler, P. M.; Williamson, C.; Wimmer, D.; Ye, P. L.; Baltensperger, U.; Carslaw, K. S.; Kulmala, M.; Worsnop, D. R.; Curtius, J. Neutral Molecular Cluster Formation of Sulfuric Acid-Dimethylamine Observed in Real Time under Atmospheric Conditions. *Proc. Natl. Acad. Sci. U. S. A.* **2014**, *111* (42), 15019–15024. https://doi.org/10.1073/pnas.1404853111.

(33) Stark, H.; Yatavelli, R. L. N.; Thompson, S. L.; Kang, H.; Krechmer, J. E.; Kimmel, J. R.; Palm, B. B.; Hu, W. W.; Hayes, P. L.; Day, D. A.; Campuzano-Jost, P.; Canagaratna, M. R.; Jayne, J. T.; Worsnop, D. R.; Jimenez, J. L. Impact of Thermal Decomposition on Thermal Desorption Instruments: Advantage of Thermogram Analysis for Quantifying Volatility Distributions of Organic Species. *Environ. Sci. Technol.* **2017**, *51*, 8491–8500. https://doi.org/10.1021/acs.est.7b00160.

(34) Wang, M. Y.; Yao, L.; Zheng, J.; Wang, X. K.; Chen, J. M.; Yang, X.; Worsnop, D. R.; Donahue, N. M.; Wang, L. Reactions of Atmospheric Particulate Stabilized Criegee Intermediates Lead to High-Molecular-Weight Aerosol Components. *Environ. Sci. Technol.* **2016**, *50*, 5702–5710. https://doi.org/10.1021/acs.est.6b02114.

(35) Donahue, N. M.; Epstein, S. A.; Pandis, S. N.; Robinson, A. L. A Two-Dimensional Volatility Basis Set: 1. Organic-Aerosol Mixing Thermodynamics. *Atmos. Chem. Phys.* **2011**, *11* (7), 3303–3318. https://doi.org/10.5194/acp-11-3303-2011.

(36) Schervish, M.; Donahue, N. M. Peroxy Radical Chemistry and the Volatility Basis Set. *Atmos. Chem. Phys.* **2020**, *20*, 1183–1199. https://doi.org/10.5194/acp-20-1183-2020.

(37) Bianchi, F.; Kurtén, T.; Riva, M.; Mohr, C.; Rissanen, M. P.; Roldin, P.; Berndt, T.; Crounse, J. D.; Wennberg, P. O.; Mentel, T. F.; Wildt, J.; Junninen, H.; Jokinen, T.; Kulmala, M.; Worsnop, D. R.; Thornton, J. A.; Donahue, N.; Kjaergaard, H. G.; Ehn, M. Highly Oxygenated Organic Molecules (HOM)

from Gas-Phase Autoxidation Involving Peroxy Radicals: A Key Contributor to Atmospheric Aerosol. *Chem. Rev.* **2019**, *119* (6), 3472–3509. https://doi.org/10.1021/acs.chemrev.8b00395.

(38) Emanuelsson, E. U.; Hallquist, M.; Kristensen, K.; Glasius, M.; Bohn, B.; Fuchs, H.; Kammer, B.; Kiendler-Scharr, A.; Nehr, S.; Rubach, F.; Tillmann, R.; Wahner, A.; Wu, H.-C. C.; Mentel, T. F. Formation of Anthropogenic Secondary Organic Aerosol (SOA) and Its Influence on Biogenic SOA Properties. *Atmos. Chem. Phys.* **2013**, *13* (5), 2837–2855. https://doi.org/10.5194/acp-13-2837-2013.

(39) Pankow, J. F.; Asher, W. E. SIMPOL.1: A Simple Group Contribution Method for Predicting Vapor Pressures and Enthalpies of Vaporization of Multifunctional Organic Compounds. *Atmos. Chem. Phys.* **2008**, *8*, 2773–2796. https://doi.org/DOI 10.5194/acp-8-2773-2008.

(40) Bilde, M.; Barsanti, K.; Booth, M.; Cappa, C. D.; Donahue, N. M.; Emanuelsson, E. U.; McFiggans, G.; Krieger, U. K.; Marcolli, C.; Topping, D.; Ziemann, P.; Barley, M.; Clegg, S.; Dennis-Smither, B.; Hallquist, M.; Hallquist, Å. M.; Khlystov, A.; Kulmala, M.; Mogensen, D.; Percival, C. J.; Pope, F.; Reid, J. P.; Ribeiro da Silva, M. A. V; Rosenoern, T.; Salo, K.; Soonsin, V. P.; Yli-Juuti, T.; Prisle, N. L.; Pagels, J.; Rarey, J.; Zardini, A. A.; Riipinen, I. Saturation Vapor Pressures and Transition Enthalpies of Low-Volatility Organic Molecules of Atmospheric Relevance: From Dicarboxylic Acids to Complex Mixtures. *Chem. Rev.* **2015**, *115* (10), 4115–4156. https://doi.org/10.1021/cr5005502.

(41) Wu, R. R.; Pan, S. S.; Li, Y.; Wang, L. M. Atmospheric Oxidation Mechanism of Toluene. *J. Phys. Chem. A* **2014**, *118* (25), 4533–4547. https://doi.org/10.1021/jp500077f.

(42) Wang, S. N.; Wu, R. R.; Berndt, T.; Ehn, M.; Wang, L. M. Formation of Highly Oxidized Radicals and Multifunctional Products from the Atmospheric Oxidation of Alkylbenzenes. *Environ. Sci. Technol.* **2017**, *51*, 8442–8449. https://doi.org/10.1021/acs.est.7b02374.

(43) Volkamer, R.; Platt, U.; Wirtz, K. Primary and Secondary Glyoxal Formation from Aromatics: Experimental Evidence for the Bicycloalkyl - Radical Pathway from Benzene, Toluene, and p-Xylene. *J. Phys. Chem. A* **2001**, *105* (33), 7865–7874. https://doi.org/10.1021/jp010152w.

(44) Ji, Y. M.; Zhao, J.; Terazono, H.; Misawa, K.; Levitt, N. P.; Li, Y. X.; Lin, Y.; Peng, J. F.; Wang, Y.; Duan, L.; Pan, B. W.; Zhang, F.; Feng, X. D.; An, T. C.; Marrero-Ortiz, W.; Secrest, J.; Zhang, A. L.; Shibuya, K.; Molina, M. J.; Zhang, R. Y. Reassessing the Atmospheric Oxidation Mechanism of Toluene. *Proc. Natl. Acad. Sci. U. S. A.* **2017**, *114*, 8169–8174. https://doi.org/10.1073/pnas.1705463114.

(45) Klotz, B.; Sørensen, S.; Barnes, I.; Becker, K. H.; Etzkorn, T.; Volkamer, R.; Platt, U.; Wirtz, K.; Martin-Reviejo, M. Atmospheric Oxidation of Toluene in a Large-Volume Outdoor Photoreactor: In Situ

Determination of Ring-Retaining Product Yields. *J. Phys. Chem. A* **1998**, *102* (50), 10289–10299. https://doi.org/10.1021/jp982719n.

(46) Olariu, R. I.; Klotz, B.; Barnes, I.; Becker, K. H.; Mocanu, R. FT-IR Study of the Ring-Retaining Products from the Reaction of OH Radicals with Phenol, o-, m-, and p-Cresol. *Atmos. Environ.* **2002**, *36* (22), 3685–3697. https://doi.org/Pii S1352-2310(02)00202-9 Doi 10.1016/S1352-2310(02)00202-9.

(47) Schwantes, R. H.; Schilling, K. A.; McVay, R. C.; Lignell, H.; Coggon, M. M.; Zhang, X.; Wennberg, P. O.; Seinfeld, J. H. Formation of Highly Oxygenated Low-Volatility Products from Cresol Oxidation. *Atmos. Chem. Phys.* **2017**, *17* (5), 3453–3474. https://doi.org/10.5194/acp-17-3453-2017.

(48) Iyer, S.; Lopez-Hilfiker, F.; Lee, B. H.; Thornton, J. A.; Kurtén, T.; Kurten, T. Modeling the Detection of Organic and Inorganic Compounds Using Iodide-Based Chemical Ionization. *J. Phys. Chem. A* **2016**, *120* (4), 576–587. https://doi.org/10.1021/acs.jpca.5b09837.

(49) Zhao, B.; Wang, S.; Donahue, N. M.; Chuang, W.; Hildebrandt Ruiz, L.; Ng, N. L.; Wang, Y.; Hao, J. Evaluation of One-Dimensional and Two-Dimensional Volatility Basis Sets in Simulating the Aging of Secondary Organic Aerosol with Smog-Chamber Experiments. *Environ. Sci. Technol.* **2015**, *49* (4), 2245–2254. https://doi.org/10.1021/es5048914.

(50) Zhao, B.; Wang, S.; Donahue, N. M.; Jathar, S. H.; Huang, X.; Wu, W.; Hao, J.; Robinson, A. L. Quantifying the Effect of Organic Aerosol Aging and Intermediate-Volatility Emissions on Regional-Scale Aerosol Pollution in China. *Sci. Rep.* **2016**, *6* (June), 28815. https://doi.org/10.1038/srep28815.

(51) Donahue, N. M.; Chuang, W.; Epstein, S. A.; Kroll, J. H.; Worsnop, D. R.; Robinson, A. L.; Adams, P. J.; Pandis, S. N. Why Do Organic Aerosols Exist? Understanding Aerosol Lifetimes Using the Two-Dimensional Volatility Basis Set. *Environ. Chem.* **2013**, *10*, 151–157.

(52) Riccobono, F.; Schobesberger, S.; Scott, C. E.; Dommen, J.; Ortega, I. K.; Rondo, L.; Almeida, J.; Amorim, A.; Bianchi, F.; Breitenlechner, M.; David, A.; Downard, A.; Dunne, E. M.; Duplissy, J.; Ehrhart, S.; Flagan, R. C.; Franchin, A.; Hansel, A.; Junninen, H.; Kajos, M.; Keskinen, H.; Kupc, A.; Kurten, A.; Kvashin, A. N.; Laaksonen, A.; Lehtipalo, K.; Makhmutov, V.; Mathot, S.; Nieminen, T.; Onnela, A.; Petaja, T.; Praplan, A. P.; Santos, F. D.; Schallhart, S.; Seinfeld, J. H.; Sipila, M.; Spracklen, D. V.; Stozhkov, Y.; Stratmann, F.; Tome, A.; Tsagkogeorgas, G.; Vaattovaara, P.; Viisanen, Y.; Vrtala, A.; Wagner, P. E.; Weingartner, E.; Wex, H.; Wimmer, D.; Carslaw, K. S.; Curtius, J.; Donahue, N. M.; Kirkby, J.; Kulmala, M.; Worsnop, D. R.; Baltensperger, U.; Kürten, A.; Kvashin, A. N.; Laaksonen, A.; Lehtipalo, K.; Makhmutov, V.; Mathot, S.; Nieminen, T.; Onnela, A.; Petäjä, T.; Praplan, A. P.; Santos,

F. D.; Schallhart, S.; Seinfeld, J. H.; Sipilä, M.; Spracklen, D. V.; Stozhkov, Y.; Stratmann, F.; Tomé, A.; Tsagkogeorgas, G.; Vaattovaara, P.; Viisanen, Y.; Vrtala, A.; Wagner, P. E.; Weingartner, E.; Wex, H.; Wimmer, D.; Carslaw, K. S.; Curtius, J.; Donahue, N. M.; Kirkby, J.; Kulmala, M.; Worsnop, D. R.; Baltensperger, U. Oxidation Products of Biogenic Emissions Contribute to Nucleation of Atmospheric Particles. *Science (80-.).* **2014**, *344*, 717–721. https://doi.org/10.1126/science.1243527.

(53) Nieminen, T.; Lehtinen, K. E. J.; Kulmala, M. Sub-10 Nm Particle Growth by Vapor Condensation – Effects of Vapor Molecule Size and Particle Thermal Speed. *Atmos. Chem. Phys.* **2010**, *10* (20), 9773–9779. https://doi.org/10.5194/acp-10-9773-2010.

705 **FIGURE LEGENDS**

706

707 **Figure 1.** Directly measured particle-phase oxidation products plotted on a two-dimensional
708 VBS. The background colors indicate the saturation concentration (C^*) range of ultra-low
709 volatility (ULVOCs, purple), extremely low volatility (ELVOCs, gray), low volatility (LVOCs,
710 pink) and semi-volatile (SVOCs, green) organic compounds. (*A*) Monomers (crosses) and
711 dimers (dots) from toluene (blue symbols) and naphthalene (gray symbols) photo-oxidation
712 with NO_x present. The volatility distribution can be represented by carbon numbers isopleths
713 (red dashed lines) derived from the original volatility basis set (VBS) parameterization [35]. (*B*)
714 Monomers (green crosses) and dimers (green dots) from α-pinene ozonolysis with NO_x present
715 observed in CLOUD 11 experiments as well as carbon numbers isopleths (black dashed lines)
716 calculated using a revised VBS parameterization to reflect the –OOH functionality formed via
717 autoxidation [9]. (*C*) Direct comparison of aromatic-derived dimers and α-pinene-derived dimers.
718 Both are C_{20} but the aromatics are much less volatile than α-pinene-derived dimers. Symbol
719 sizes are proportional to the particle-phase signals.

720

721 **Figure 2.** Directly measured volatility distributions of particle-phase products formed during
722 toluene (*A*) and naphthalene (*B*) photo-oxidation with NO_x present. Products are binned with
723 the measured relative mass concentration in percent. The measured oxidation products are
724 divided into organonitrate monomers (light blue), pure organic monomers (light green),
725 organonitrate dimers (navy blue) and pure organic dimers (dark green). (*C*) Growth rates
726 measured with DMA train vs the sum of sulfuric acid and HOM concentrations. Sulfuric acid
727 kinetic limit is taken from Nieminen *et al.* [53].

728

729 **Figure 3.** The mass defect plot showing products from toluene oxidation measured in the gas
730 phase. The *x*-axis is the exact mass of oxidation products and *y*-axis is the mass defect. The
731 color of circles denotes the type of products, and their size is proportional to the logarithm of
732 the count rate. Each straight line represents a group of compounds with the same number of
733 carbon, hydrogen, and nitrogen atoms, but a different number of oxygen atoms.

734

735 **Figure 4.** Gas-phase chemical mechanism for toluene photo-oxidation with NO_x present. The
736 reaction starts with OH addition to the aromatic ring, resulting in oxidized radicals. Closed-
737 shell products will be formed after radicals undergo various termination pathways. Products
738 outlined are detected by the iodide-adduct CIMS. Non-nitrate products and organonitrate
739 products are marked with green and blue, respectively. (Adapted from Schwantes *et al.* [47].)
740

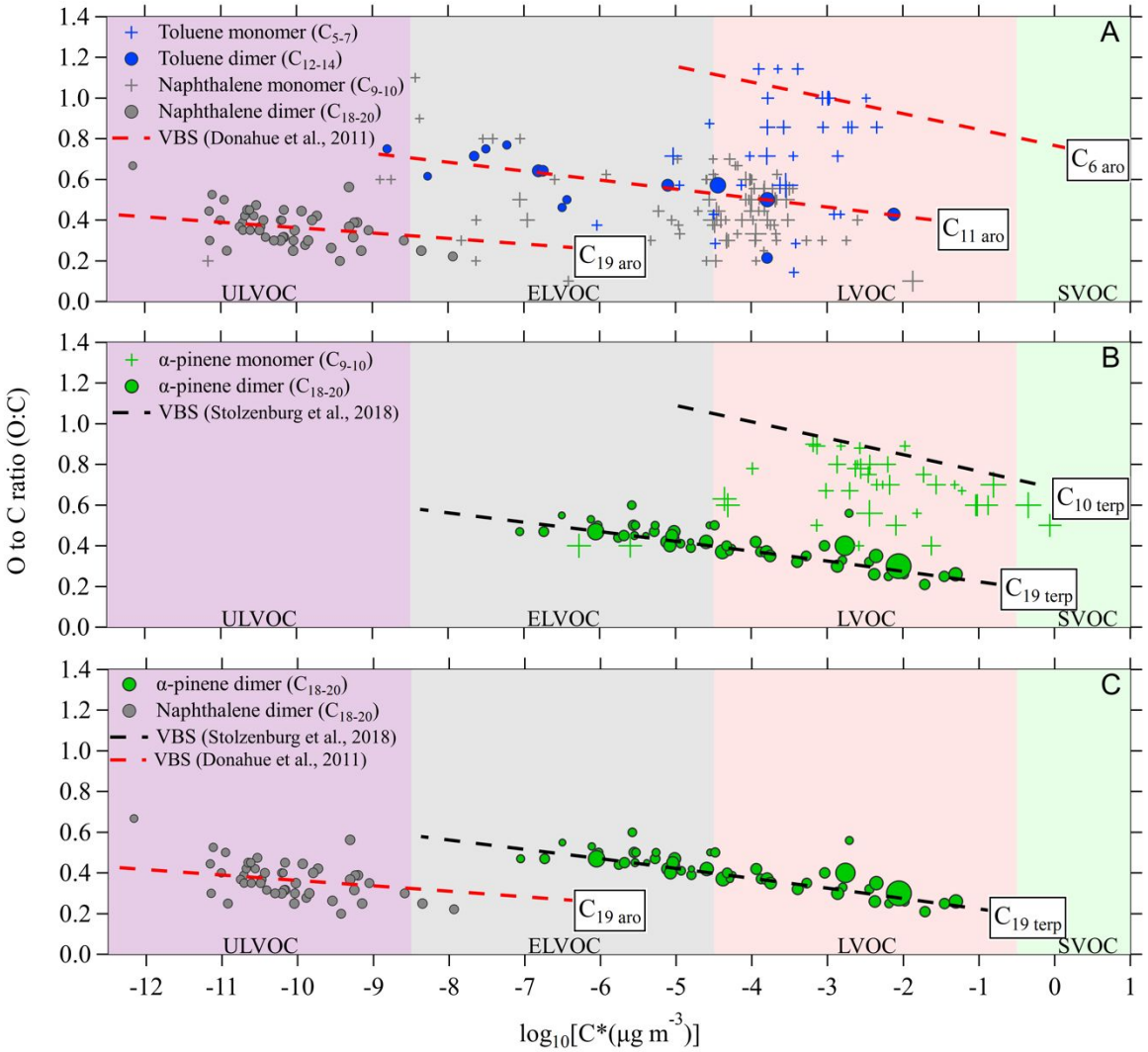

741

742

743 **Figure 1.**

744

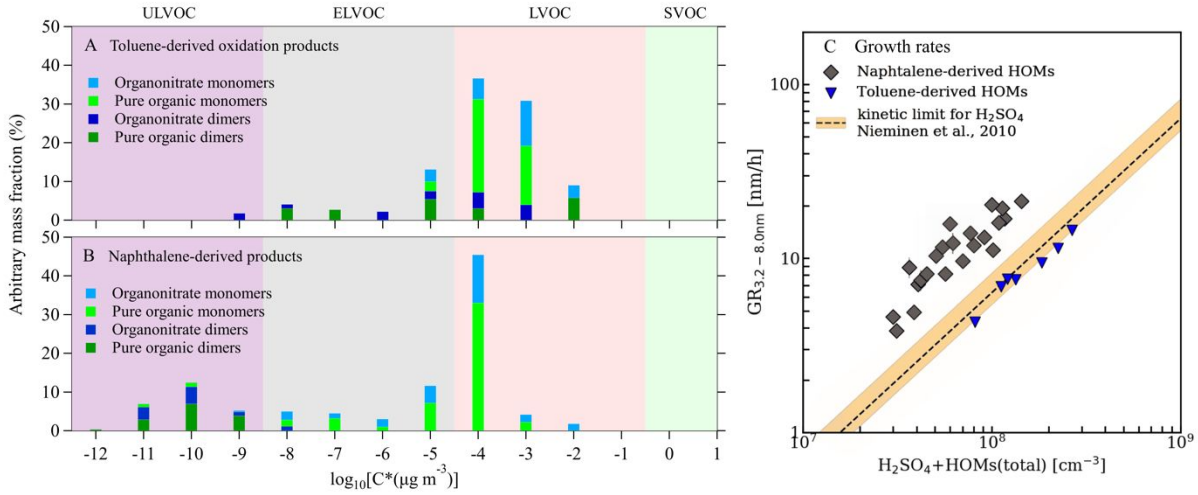

745

746

747 **Figure 2.**

748

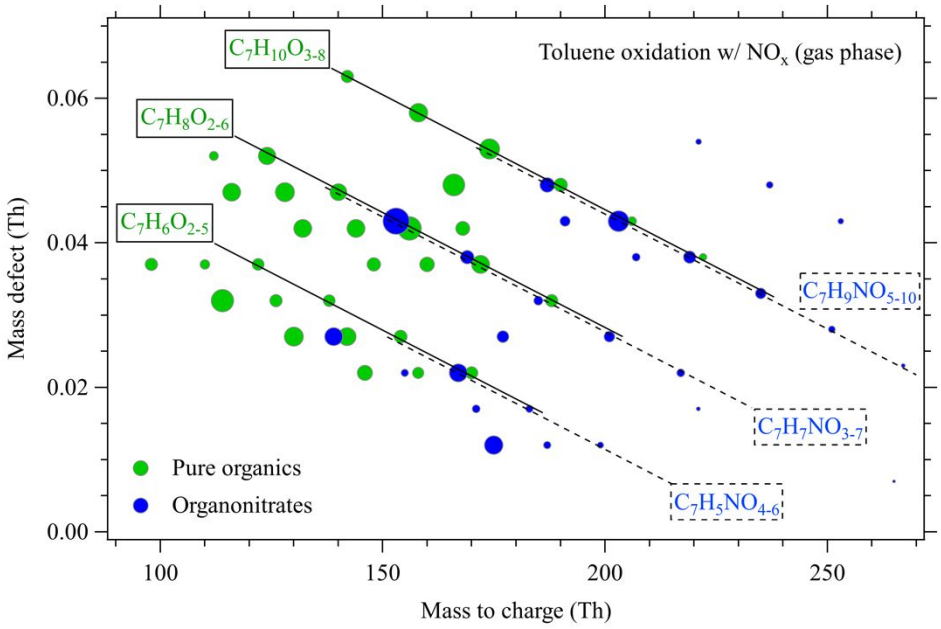

749

750

751 **Figure 3.**

752

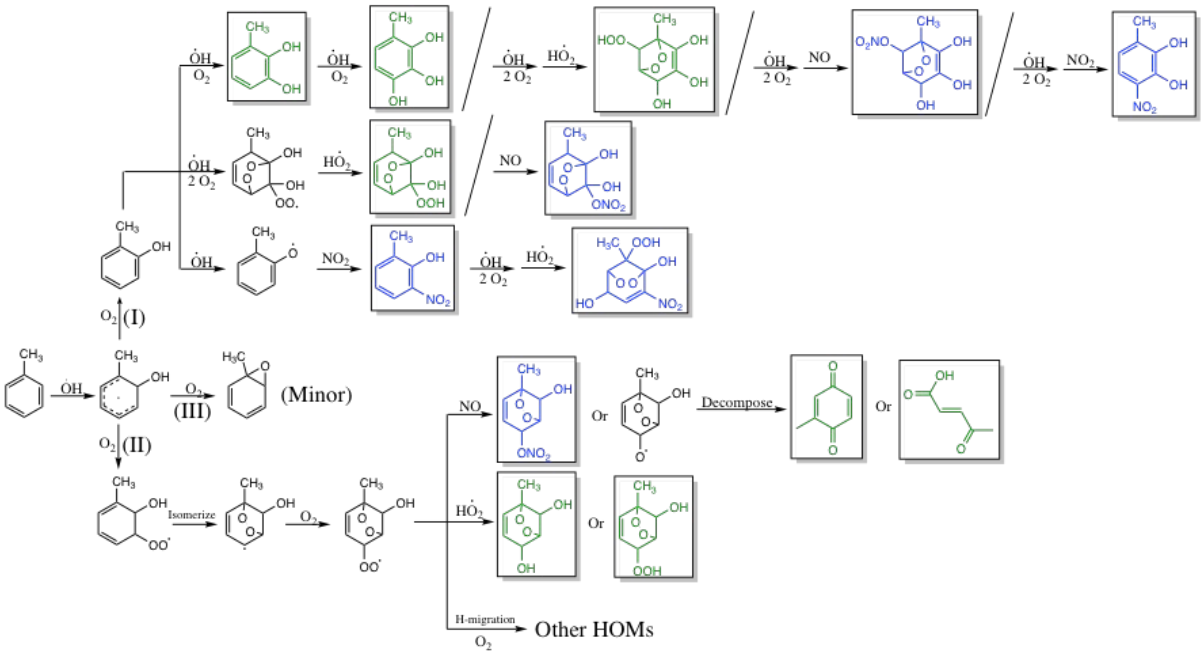
(I)
(II)
(III)
(Minor)
Isomerize
Decompose
Or
Other HOMs
H-migration

Figure 4.

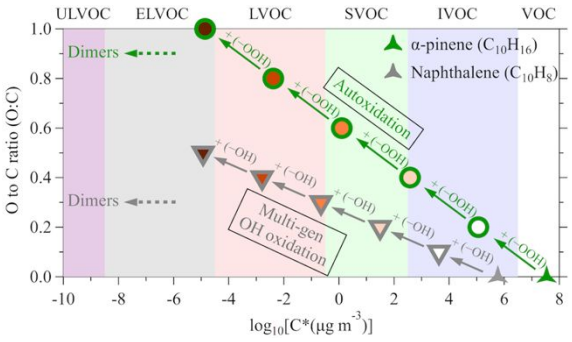
ULVOC
ELVOC
LVOC
SVOC
IVOC
VOC
α-pinene ($C_{10}H_{16}$)
Naphthalene ($C_{10}H_8$)
Dimers
Dimers
Autoxidation
Multi-gen OH oxidation
+(-OOH)
+(-OH)
O to C ratio (O:C)
$\log_{10}$[C*(μg m^{-3})]

TOC art

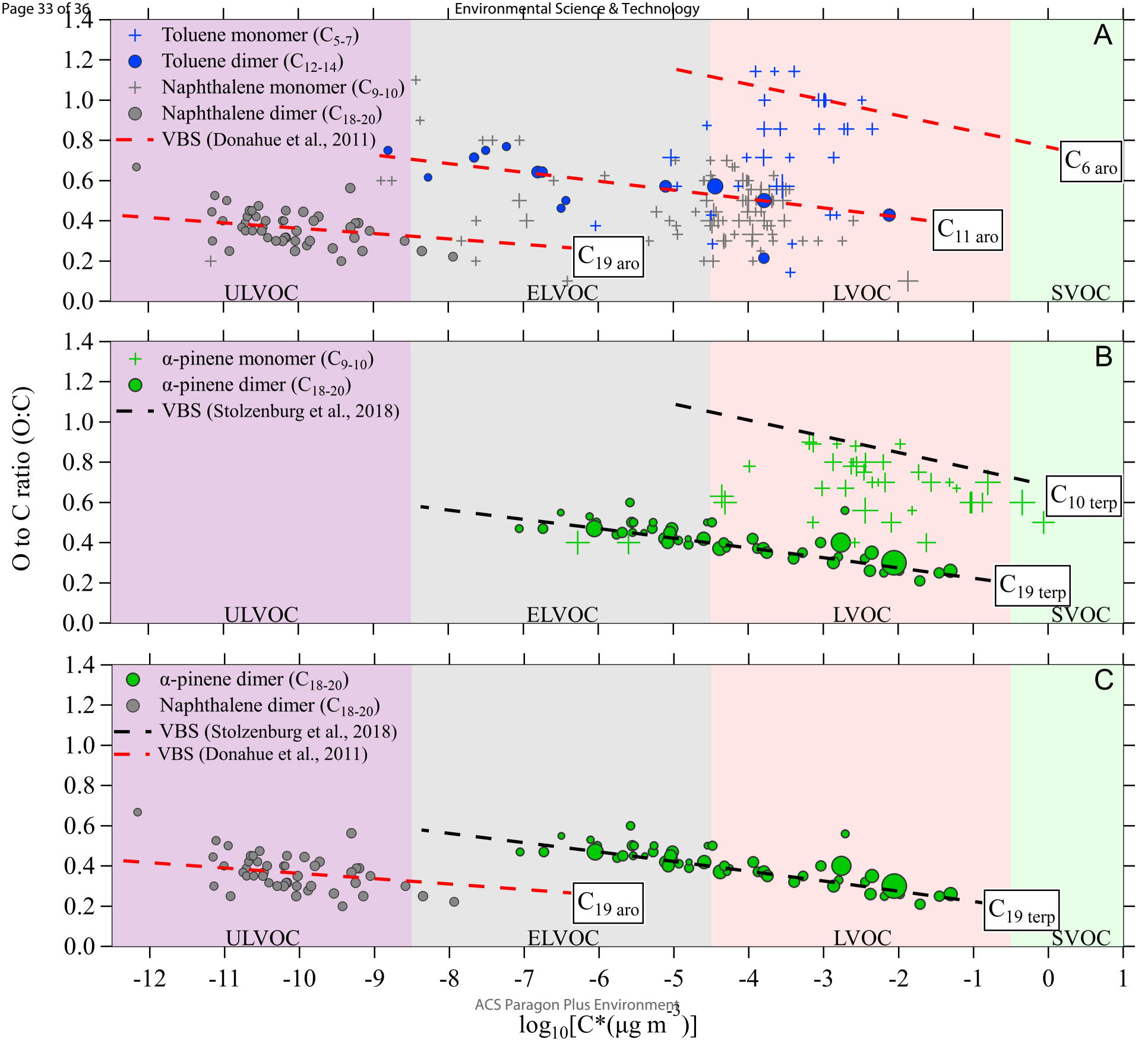
A
Toluene monomer (C_{5-7})
Toluene dimer (C_{12-14})
Naphthalene monomer (C_{9-10})
Naphthalene dimer (C_{18-20})
VBS (Donahue et al., 2011)
$C_{6\ aro}$
$C_{11\ aro}$
$C_{19\ aro}$
ULVOC
ELVOC
LVOC
SVOC
B
α-pinene monomer (C_{9-10})
α-pinene dimer (C_{18-20})
VBS (Stolzenburg et al., 2018)
$C_{10\ terp}$
$C_{19\ terp}$
C
α-pinene dimer (C_{18-20})
Naphthalene dimer (C_{18-20})
VBS (Stolzenburg et al., 2018)
VBS (Donahue et al., 2011)
$C_{19\ aro}$
$C_{19\ terp}$
O to C ratio (O:C)
$\log_{10}[C^*(\mu g\ m^{-3})]$

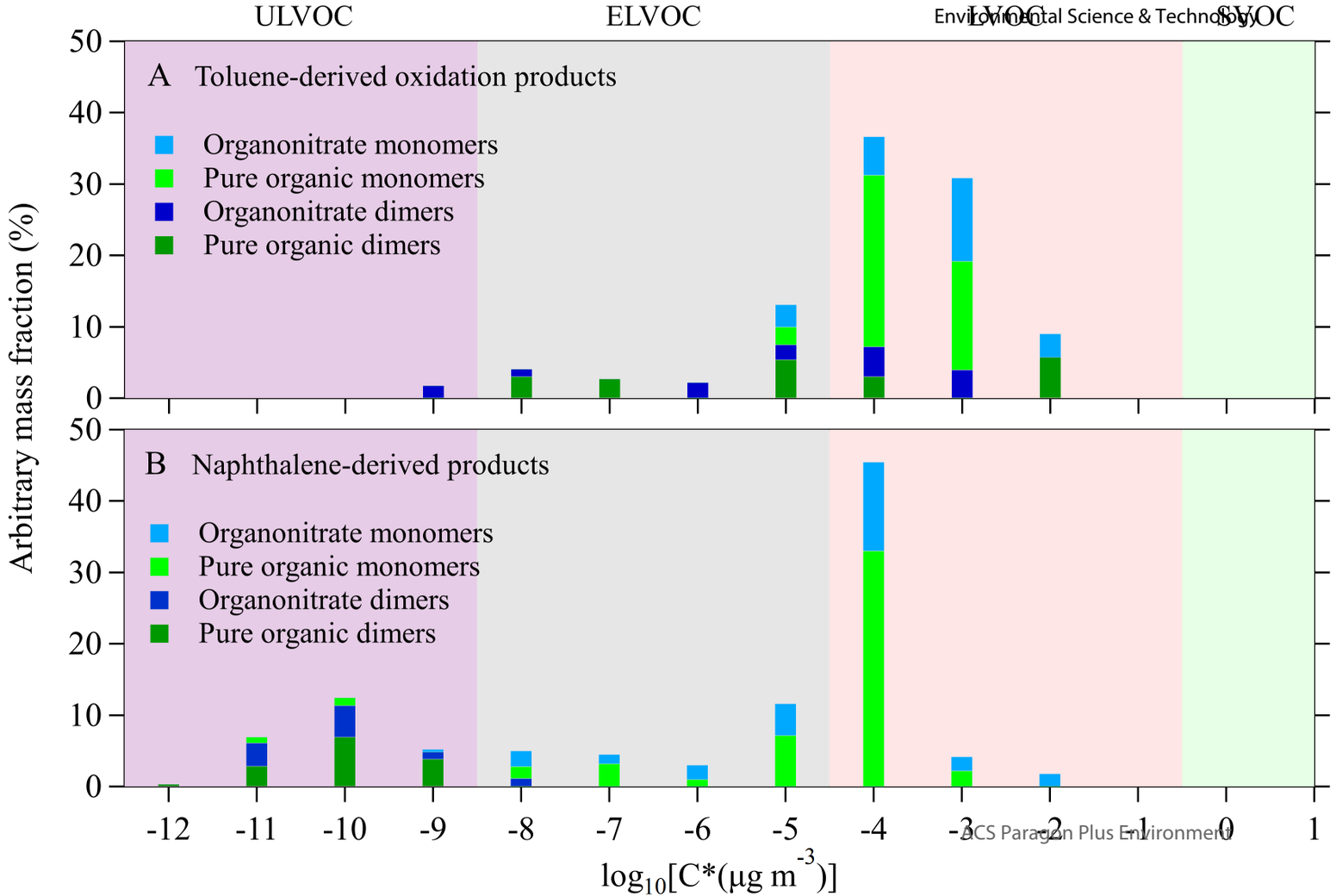

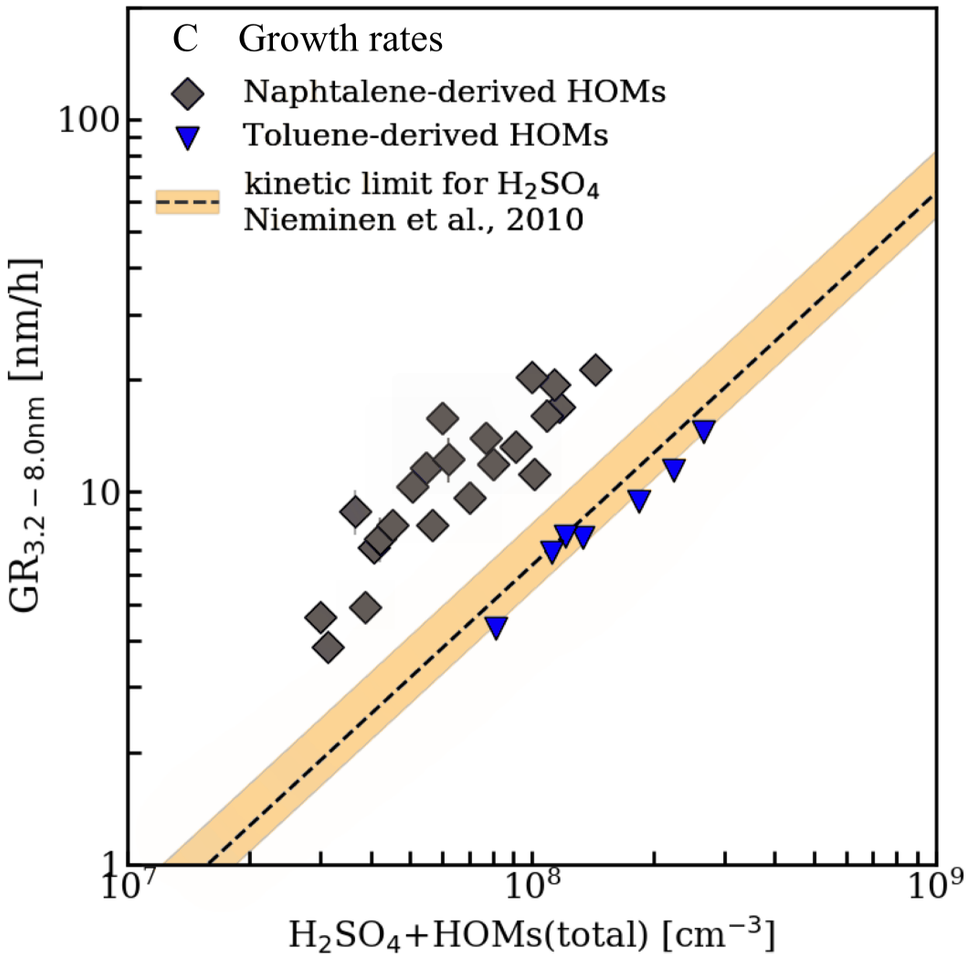

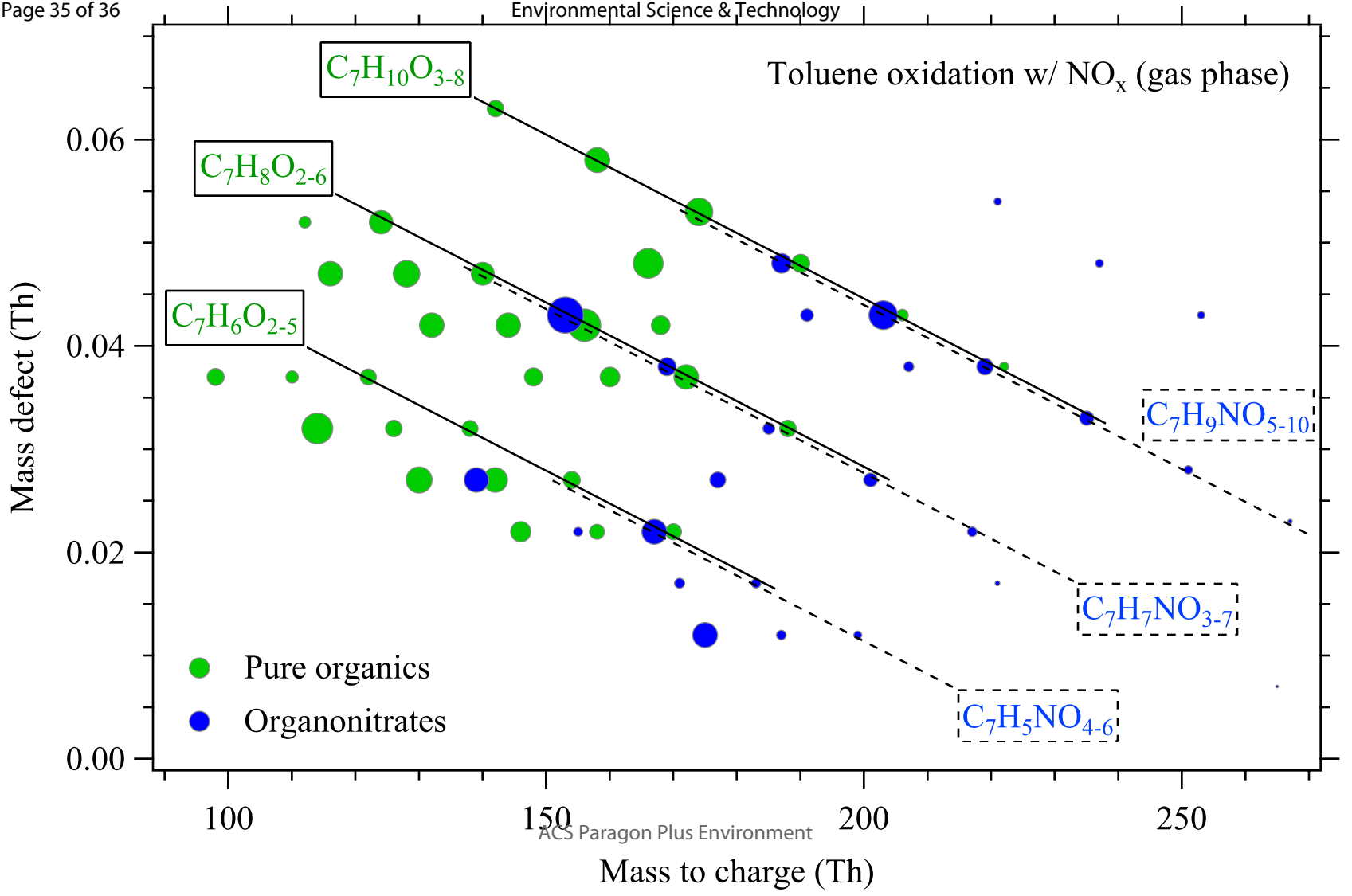
Toluene oxidation w/ NO_x (gas phase)
$C_7H_{10}O_{3-8}$
$C_7H_8O_{2-6}$
$C_7H_6O_{2-5}$
$C_7H_9NO_{5-10}$
$C_7H_7NO_{3-7}$
$C_7H_5NO_{4-6}$
Pure organics
Organonitrates
Mass defect (Th)
0.00
0.02
0.04
0.06
100
150
200
250
Mass to charge (Th)

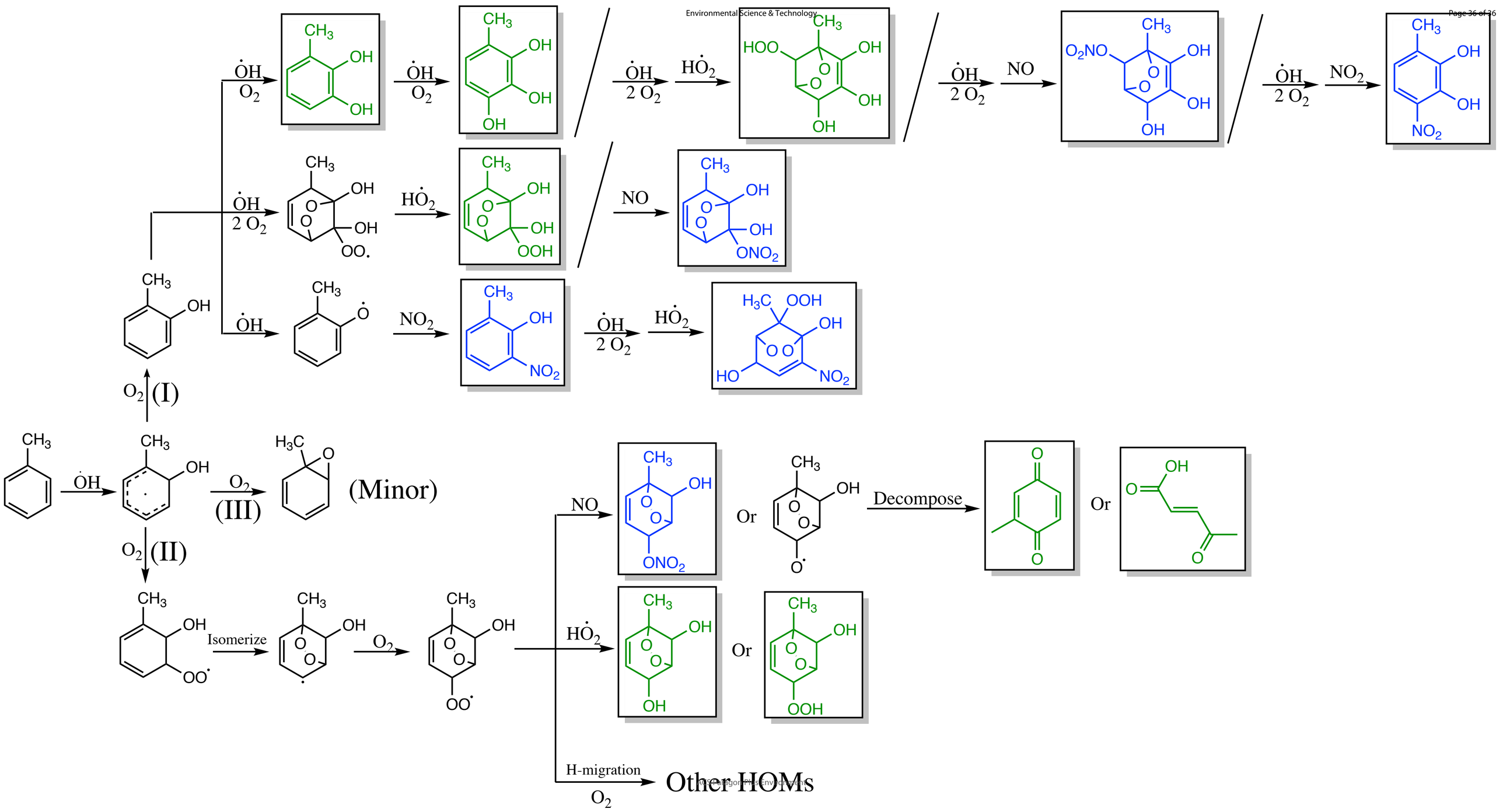

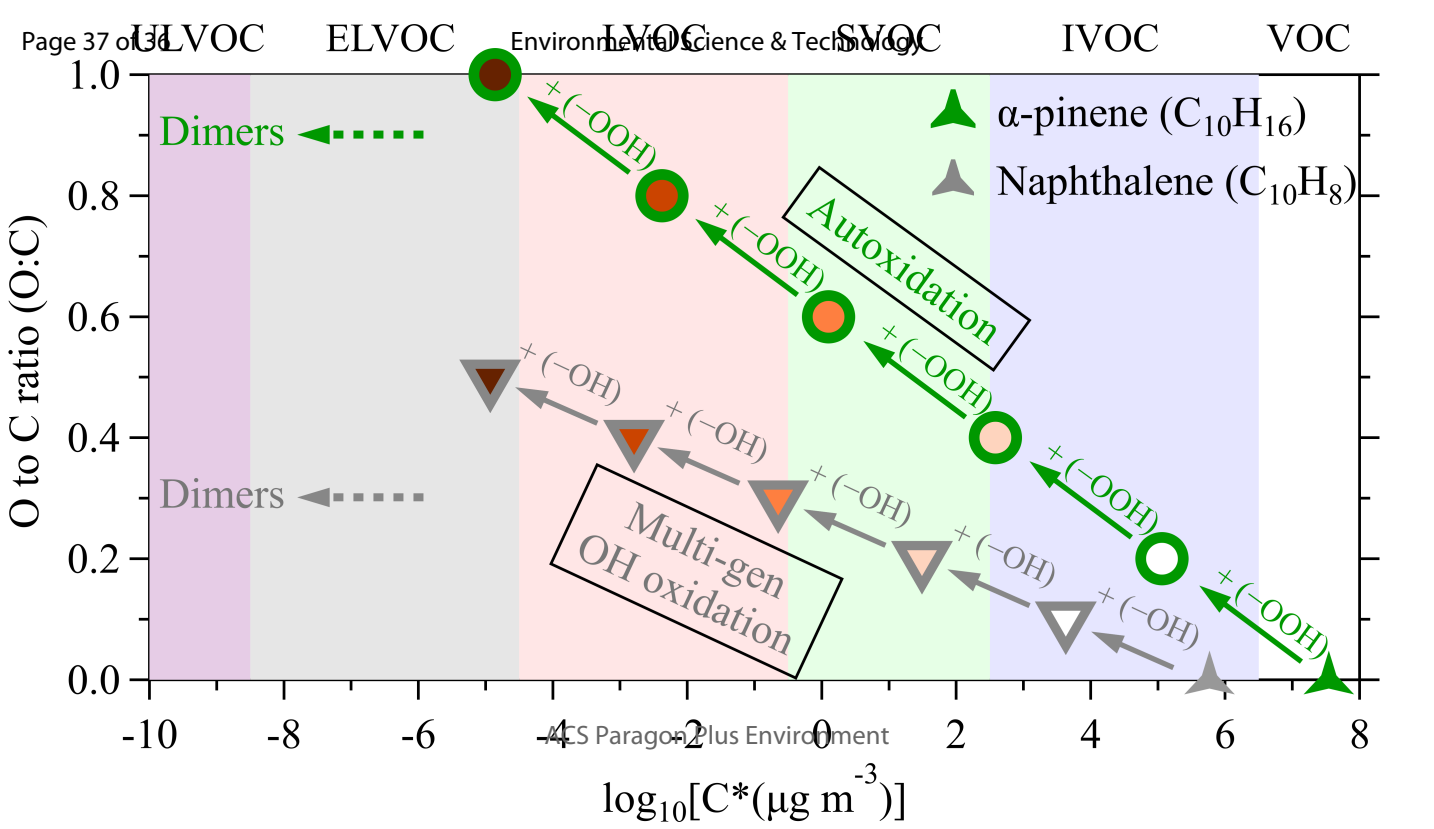
ULVOC
ELVOC
LVOC
SVOC
IVOC
VOC
α-pinene ($C_{10}H_{16}$)
Naphthalene ($C_{10}H_8$)
Dimers
Dimers
Autoxidation
Multi-gen OH oxidation
+(−OOH)
+(−OH)
O to C ratio (O:C)
$\log_{10}[C^*(\mu g\ m^{-3})]$
ACS Paragon Plus Environment